NASA/TM-2006-213674

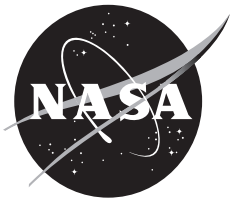

The F-15B Lifting Insulating Foam Trajectory (LIFT) Flight Test

Stephen Corda, Donald Whiteman, Ting Tseng
NASA Dryden Flight Research Center
Edwards, California

Ricardo Machin
NASA Johnson Space Center
Houston, Texas

June 2006

NASA STI Program ... in Profile

Since its founding, NASA has been dedicated to the advancement of aeronautics and space science. The NASA scientific and technical information (STI) program plays a key part in helping NASA maintain this important role.

The NASA STI program is operated under the auspices of the Agency Chief Information Officer. It collects, organizes, provides for archiving, and disseminates NASA's STI. The NASA STI program provides access to the NASA Aeronautics and Space Database and its public interface, the NASA Technical Report Server, thus providing one of the largest collections of aeronautical and space science STI in the world. Results are published in both non-NASA channels and by NASA in the NASA STI Report Series, which includes the following report types:

- TECHNICAL PUBLICATION. Reports of completed research or a major significant phase of research that present the results of NASA programs and include extensive data or theoretical analysis. Includes compilations of significant scientific and technical data and information deemed to be of continuing reference value. NASA counterpart of peer-reviewed formal professional papers but has less stringent limitations on manuscript length and extent of graphic presentations.

- TECHNICAL MEMORANDUM. Scientific and technical findings that are preliminary or of specialized interest, e.g., quick release reports, working papers, and bibliographies that contain minimal annotation. Does not contain extensive analysis.

- CONTRACTOR REPORT. Scientific and technical findings by NASA-sponsored contractors and grantees.

- CONFERENCE PUBLICATION. Collected papers from scientific and technical conferences, symposia, seminars, or other meetings sponsored or cosponsored by NASA.

- SPECIAL PUBLICATION. Scientific, technical, or historical information from NASA programs, projects, and missions, often concerned with subjects having substantial public interest.

- TECHNICAL TRANSLATION. English-language translations of foreign scientific and technical material pertinent to NASA's mission.

Specialized services also include creating custom thesauri, building customized databases, and organizing and publishing research results.

For more information about the NASA STI program, see the following:

Access the NASA STI program home page at *http://www.sti.nasa.gov*.

- E-mail your question via the Internet to help@sti.nasa.gov.

- Fax your question to the NASA STI Help Desk at (301) 621-0134.

- Phone the NASA STI Help Desk at (301) 621-0390.

- Write to:
  NASA STI Help Desk
  NASA Center for AeroSpace Information
  7121 Standard Drive
  Hanover, MD 21076-1320

NASA/TM-2006-213674

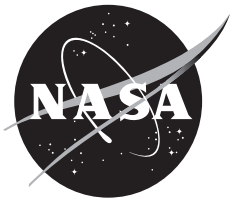

The F-15B Lifting Insulating Foam Trajectory (LIFT) Flight Test

Stephen Corda, Donald Whiteman, Ting Tseng
NASA Dryden Flight Research Center
Edwards, California

Ricardo Machin
NASA Johnson Space Center
Houston, Texas

National Aeronautics and
Space Administration

Dryden Flight Research Center
Edwards, California 93523-0273

June 2006

NOTICE

Use of trade names or names of manufacturers in this document does not constitute an official endorsement of such products or manufacturers, either expressed or implied, by the National Aeronautics and Space Administration.

Available from the following:

NASA Center for AeroSpace Information
7121 Standard Drive
Hanover, MD 21076-1320
(301) 621-0390

National Technical Information Service
5285 Port Royal Road
Springfield, VA 22161-2171
(703) 605-6000

CONTENTS

TABLES

FIGURES

ABSTRACT

A series of flight tests has been performed to assess the structural survivability of space shuttle external tank debris, known as divots, in a real flight environment. The NASA F-15B research test bed aircraft carried the Aerodynamic Flight Test Fixture configured with a shuttle foam divot ejection system. The divots were released in flight at subsonic and supersonic test conditions matching points on the shuttle ascent trajectory. Very high-speed digital video cameras recorded the divot trajectories. The objectives of the flight test were to determine the structural survivability of the divots in a real flight environment, assess the aerodynamic stability of the divots, and provide divot trajectory data for comparison with debris transport models. A total of 10 flights to Mach 2 were completed, resulting in 36 successful shuttle foam divot ejections. High-speed video was obtained at 2,000 pictures per second for all of the divot ejections. The divots that were cleanly ejected remained structurally intact. The conical frustum-shaped divots tended to aerodynamically trim in both the subsonic and supersonic free-stream flow.

NOMENCLATURE

$A_{cross\text{-}section}$	divot cross-sectional area, ft^2 (m^2)
AFTF	Aerodynamic Flight Test Fixture
C_d	divot flat plate drag coefficient
C_m	divot moment coefficient
CFD	computational fluid dynamics
deg	degree
DTA	debris transport analysis
E_{cr}	energy required to compress the foam, in-lbf (J)
g	gravitational acceleration, ft/s^2 (m/s^2)
GPS	global positioning system
H	pressure altitude, ft (m)
HT	divot thickness, in.
IRIG	Inter-Range Instrumentation Group
KCAS	knots calibrated airspeed, nmi/h (m/s)
KE	divot kinetic energy, ft-lbf (J)
L	largest divot diameter, in.
lbm	pound-mass
LIFT	Lifting Insulating Foam Trajectory
M	Mach number
MEOP	maximum expected operating pressure, lbf/in^2 (N/m^2)
NPT	National Pipe Thread

pps	pictures per second
P_s	specific excess power, ft/s (m/s)
psia	pounds per square inch, absolute
q	dynamic pressure, lbf/ft^2 (N/m^2)
STS	Space Transportation System
TC	thermocouple
TPS	thermal protection system
V_{term}	divot terminal velocity, ft/s (m/s)
W	divot weight, lb (kg)
1-DOF	one-degree-of-freedom
3-D	three-dimensional
α	angle of attack, deg
β	angle of sideslip, deg
ρ_{air}	air density, slugs/ft^3 (kg/m^3)

INTRODUCTION

The loss of the Space Shuttle Columbia (STS-107), caused by debris shed from the external tank during shuttle ascent, has prompted a large effort by NASA to understand this debris transport phenomenon (ref. 1). The shuttle external tank thermal protection system (TPS) consists of a spray-on insulating foam. The TPS protects the tank from heating during shuttle ascent and reduces the formation of ice after the tank is filled with cryogenic propellants.

One of the TPS failure modes involves cohesive-adhesive strength failure of the foam. Because of imperfections in the external tank foam application, air is trapped in voids underneath the foam. During ascent, decreasing atmospheric pressure causes an increasing pressure differential in the trapped volume of air. The force caused by the pressure differential may exceed the cohesive-adhesive strength of the foam, which causes the foam piece over the air void to shed. This type of TPS foam shedding is referred to as "divoting" (fig. 1(a)), and the shed foam debris is called a "divot" (fig. 1(b)).

NASA is conducting extensive research to understand the TPS debris transport. The debris transport analysis (DTA) includes definitions of the debris geometries, release initial conditions, and locations of debris release. Maximum expected flaw or defect characteristic lengths have been determined from dissections of sprayed foam layups and actual shuttle external tanks. Based on these investigations, a typical divot has a conical frustum shape with a base diameter of many inches. Because the TPS foam density is roughly 2 lbm/ft^3 (32.04 kg/m^3), the divot mass typically is very low.

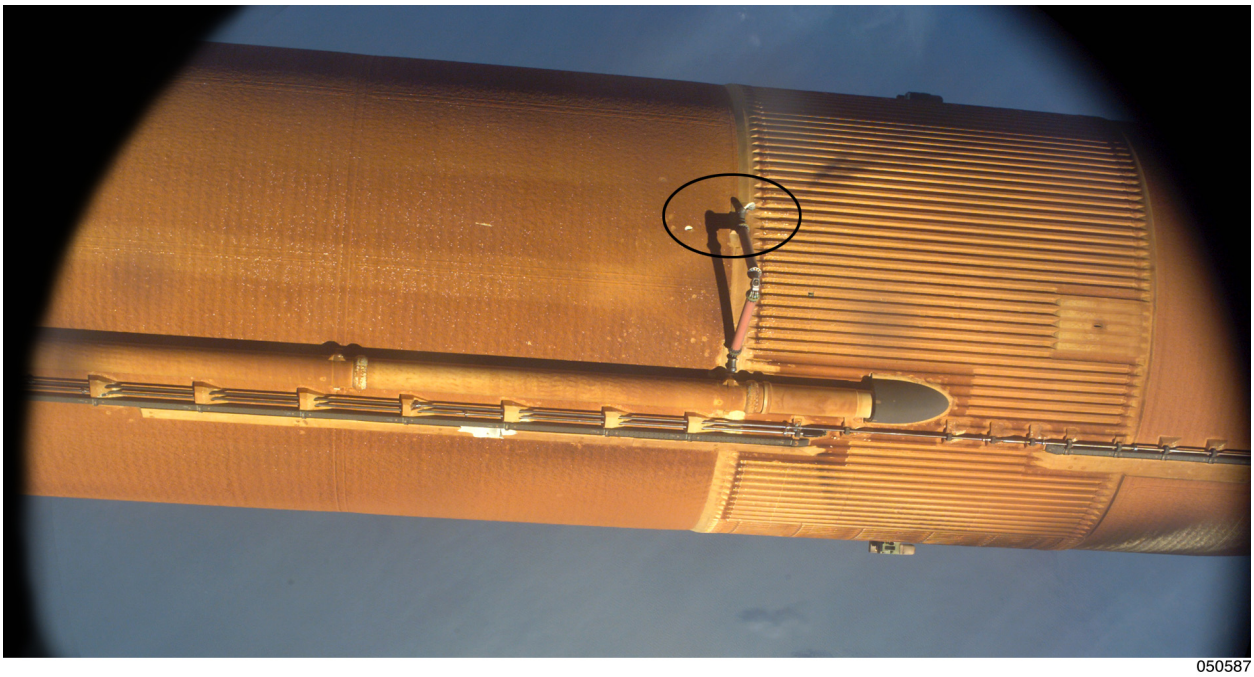

(a) Divoting near forward bipod area from STS-114.

(b) Typical shed foam debris known as a divot.

Figure 1. Cohesive-adhesive strength failure of shuttle external tank insulating foam.

From these typical divot shapes and sizes, aerodynamic and structural divot models have been developed for use in computational tools to predict the divot trajectories. To understand divot "flight" after shedding, a critical unknown must be answered: does the divot trim (that is, assume a stable orientation with respect to the free-stream flow) or tumble? The aerodynamics of the trim configuration as opposed to the tumble configuration significantly influences the divot trajectory and cross range. Ultimately this configuration translates into where the shuttle orbiter can be struck by a divot from the external tank. Another critical unknown is whether the divot remains structurally intact or fragments after release.

To obtain divot data, tests have been conducted by several means, including wind tunnel, ballistic tunnel, and flight. This report presents the results of the flight tests performed with the NASA F-15B research test bed aircraft. The F-15B aircraft carried a centerline-mounted Aerodynamic Flight Test Fixture (AFTF, previously called the Flight Test Fixture-II) configured with a divot ejection system (fig. 2). Sheets of external tank TPS foam were mounted on the side of the AFTF and back pressured to eject divots in flight at subsonic and supersonic speeds to near Mach 2.

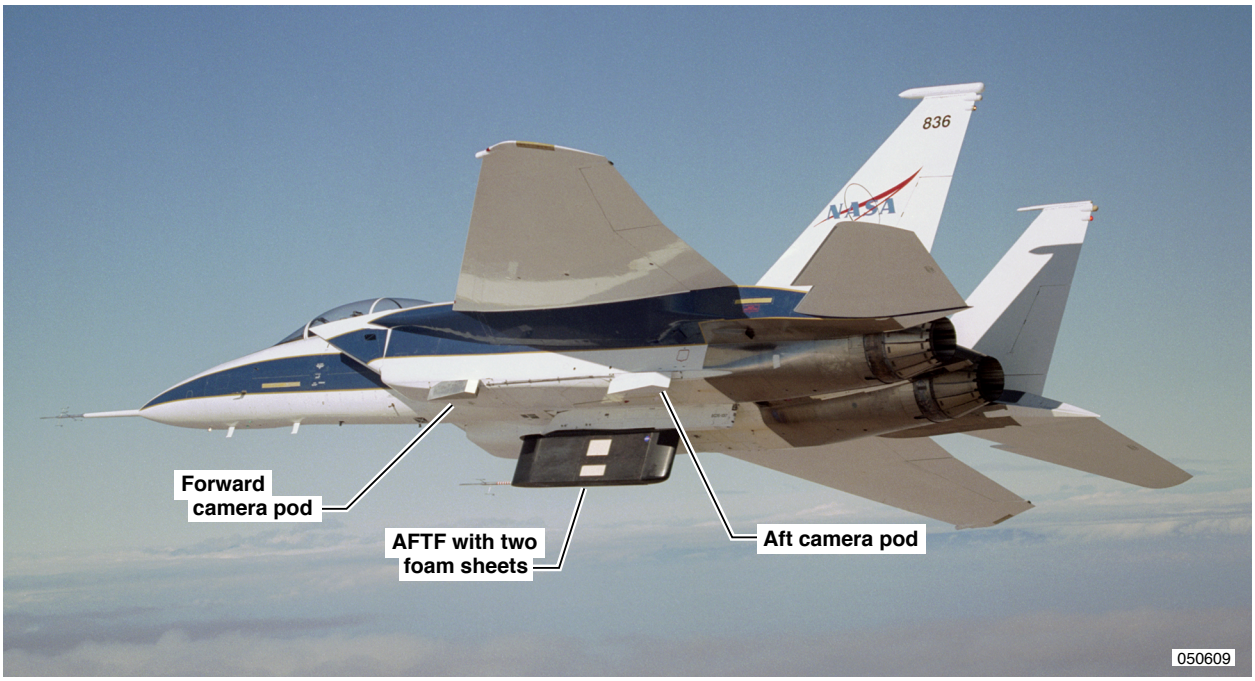

Figure 2. The NASA F-15B research test bed aircraft in flight (NASA Photo EC0030-12).

The primary objective of the flight tests was to determine the structural survivability of the divots in a real flight environment, matching the Mach number and dynamic pressure at discrete points along the shuttle ascent trajectory. Very high-speed digital video cameras were used to visually assess the structural survivability of the divot. The stability of the divot trim configuration as opposed to the divot tumble configuration also was assessed. A secondary objective was to quantify the divot trajectories through the use of photogrammetry techniques.

AIRCRAFT AND AERODYNAMIC FLIGHT TEST FIXTURE DESCRIPTIONS

The F-15B aircraft is a two-seat fighter-trainer version of the F-15A air-superiority fighter built by McDonnell Douglas Aircraft Company (now The Boeing Company, St. Louis, Missouri). The F-15B airplane has a wingspan of 42.8 ft (13.05 m), height of 18.7 ft (5.7 m) and length of 63.7 ft (19.4 m), excluding the air data nose boom (fig. 3). The aircraft has a high-mounted swept main wing with a modified delta shape, twin vertical tails, all-moving horizontal stabilators, and twin turbofan jet engines. Primary flight control surfaces are controlled by a hydromechanical system and an electrical control augmentation system (CAS). The F-15B aircraft is capable of dash speeds in excess of Mach 2 and level flight at altitudes to 60,000 ft (18,288 m).

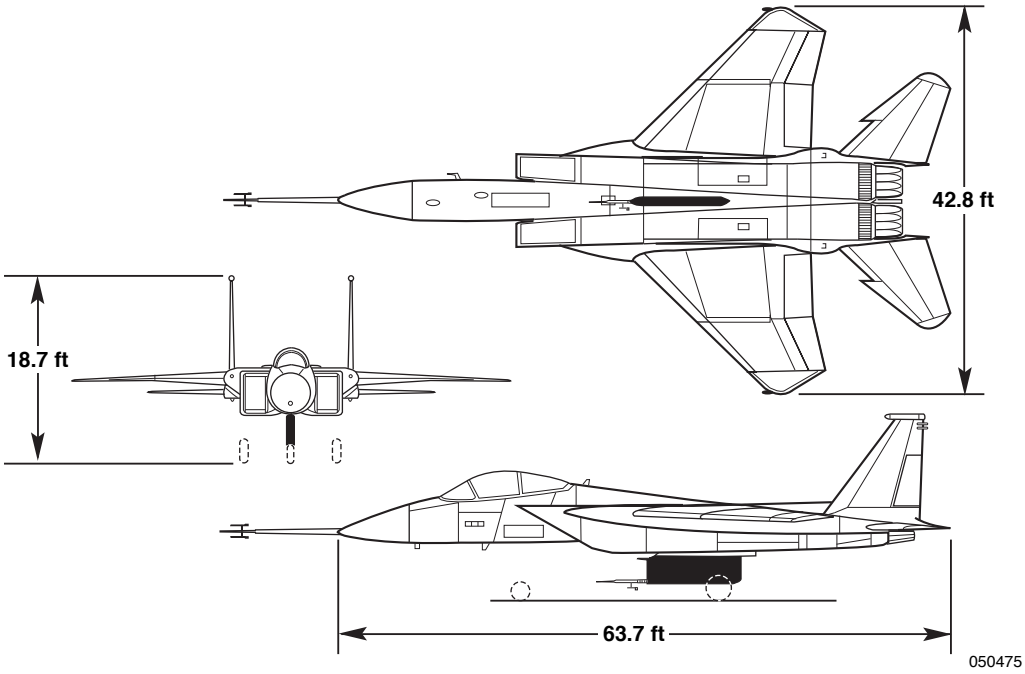

Figure 3. The NASA F-15B research test bed aircraft, shown with the Aerodynamic Flight Test Fixture and air data boom.

The F-15B aircraft is powered by two F100-PW-100 turbofan engines (Pratt & Whitney, West Palm Beach, Florida). Each engine produces an uninstalled sea level static thrust of approximately 25,000 lbf (11,340 kgf) in full afterburner. The aircraft has a fully fueled takeoff weight of approximately 42,000 lb (19,051 kg) and a landing weight of approximately 32,000 lb (14,515 kg). The aircraft has aerial refueling capability for extended-duration research missions.

Modifications made to the NASA F-15B aircraft to convert it from an air-superiority fighter to a supersonic research test bed include the installation of research systems for instrumentation, digital data recording, telemetry, in-flight video, and global positioning system (GPS) information. A significant research feature of the aircraft is the ability to carry large experiment test fixtures on the lower fuselage centerline pylon.

The AFTF is the second-generation aerodynamic flight test fixture that was built to replace the first flight test fixture flown on a NASA F-104 aircraft (refs. 2 and 3). The AFTF is a low-aspect-ratio, rectangular fin shape that is mounted underneath the aircraft on the fuselage centerline pylon (fig. 3). It has an elliptical nose section and a blunt, squared-off base. Constructed of all composite materials, the AFTF has a modular structure with four upper and four lower internal bays. The bays are accessible through removable side panels. The AFTF is 107 in. (2.718 m) long, 32 in. (0.8128 m) high, and 8 in. (0.2032 m) wide. The maximum weight is approximately 500 lb (186.6 kg). Figure 4 shows the details and dimensions of the AFTF.

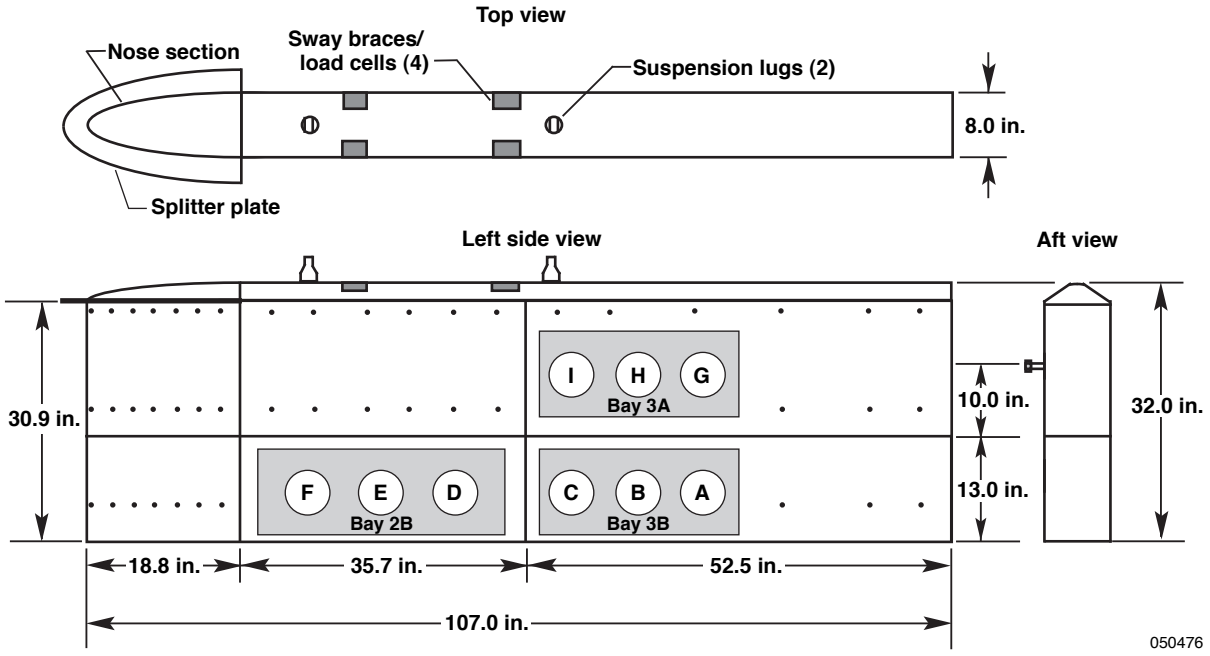

Figure 4. Details and dimensions of the Aerodynamic Flight Test Fixture.

The AFTF complements the current inventory of F-15B experimental flight test fixtures, which includes the Propulsion Flight Test Fixture (PFTF) and Centerline Instrumented Pylon (CLIP) (refs. 4 and 5). The PFTF is designed to conduct advanced propulsion experiments and the CLIP is a new fixture designed to accommodate larger span models underneath the aircraft.

Standard National Advisory Committee for Aeronautics (NACA) air data nose booms have been mounted on the F-15B airplane nose and AFTF leading edge. Each air data nose boom measures the local total pressure, static pressure, angle of attack, and angle of sideslip. Conventional flow angle vanes, mounted downstream of the static pressure ports, measure angle of attack and angle of sideslip. Total temperature is measured by probes mounted on both the airplane and AFTF aft right side. Linear and angular accelerations are measured near the centerline of the aircraft just forward and above the aircraft center of gravity.

All data were digitally recorded on board the aircraft and telemetered in real time to ground-based recorders and control room displays. Two very high-speed digital video cameras, mounted to the forward and aft fuselage missile rails, were aimed at the AFTF and monitored in the aft cockpit and control room. Data were collected continuously from takeoff to landing.

The high-speed digital video was recorded on board the aircraft. Real-time video was transmitted to the control room and displayed on the F-15B aft cockpit video monitor at a comparatively slower rate of 30 pictures per second (pps).

The telemetry system includes two telemetry transmitters and data streams, one each for the F-15B aircraft and AFTF. The F-15B telemetry system monitors aircraft instrumentation including onboard GPS, nose boom air data, and other aircraft performance and flying quality parameters. The AFTF instrumentation system provided data directly related to the Lifting Insulating Foam Trajectory (LIFT) experiment, in addition to the AFTF air data parameters. The high-speed camera system provided digital storage of video data for each divot ejection event, and data were downloaded for processing after each flight. All parameters, including the video, were correlated with onboard GPS–synchronized, Inter-Range Instrumentation Group–B (IRIG-B) timing.

The control panel for the experiment was located in the rear cockpit of the F-15B aircraft. Details of the control panel switches and operation are provided in the succeeding section, “Synchronization System.”

LIFTING INSULATING FOAM TRAJECTORY CONFIGURATION DESCRIPTION

The LIFT flight test required the development of two new systems: a very high-speed digital video camera system and a divot ejection system. These systems were developed and tested during a 3-month ground test effort preceding the flight test program.

In selecting the best divot ejection system for flight, four different systems were designed, fabricated, ground tested, and evaluated. Three of these systems, the burst disk, needle-guided pneumatic, and mechanical piston, ejected a preformed divot, whereas one system, called the pressure-failed sheet system, produced divots from a solid sheet of foam. The three systems that used a preformed divot held the divot in a cylindrical chamber and ejected it either mechanically or pneumatically.

In the burst disk system, a metal burst disk was ruptured, allowing high-pressure gas to eject the divot from the cylindrical chamber. In the needle-guided pneumatic system, the center of the divot was pierced with a thin, needle-like metal spike to help guide the divot during ejection. High-pressure gas, injected at the back of the divot by means of a simple solenoid valve system, was used to eject the divot. In the mechanical piston system, the divot was ejected by means of a piston that pushed the divot out of the cylinder. A mechanical claw was used to pressurize and release the back face of the piston.

The pressure-failed sheet system used a sheet of foam that was back pressured to produce irregularly shaped divots. This system ultimately was selected for flight because of its simplicity of operation, and because the divots were more representative of those in the actual event on the shuttle external tank.

The pressure-failed sheet divot ejection system was comprised of sheets of shuttle external tank insulating foam attached to the side of the AFTF and a nitrogen gas pneumatic system mounted inside the AFTF. Precut voids in the back of the foam sheets were pressurized with a nitrogen gas from the pneumatic system. The back pressuring of the foam sheets caused the foam to fail and created the divots that were ejected from the AFTF.

The back-pressuring mechanism used to create divots on the AFTF is similar to the actual situation on the shuttle. The foam surface temperature conditions for the AFTF are not the same as those for the shuttle. For the shuttle, the foam inner surface is exposed to cryogenic temperatures, and the foam outer surface is aerodynamically heated to high temperatures during ascent. For the AFTF, the foam inner surface was near ambient temperature during the experiment. Because the AFTF could not match the shuttle ascent trajectory, the aerodynamic heating experienced by the F-15B foam outer wall was much less than that experienced by the shuttle. Table 1 presents the AFTF foam outer wall temperatures at the test conditions.

The high-speed camera system was used to obtain digital video of the divots ejected from the AFTF. The camera heads were housed inside two camera pods mounted on the left side fuselage missile rails of the F-15B aircraft. The next section, “High-Speed Digital Video Camera System,” presents an overview of the high-speed camera and synchronization systems. Reference 6 (to be published) provides further details about the high-speed camera system.

THIS PAGE INTENTIONALLY LEFT BLANK

Table 1. The F-15B aircraft Lifting Insulating Foam Trajectory divot ejection flight test conditions and results summary.

Flight No.	Aircraft flight conditions			AFTF flight conditions					Foam Temperature	
	Mach number	Altitude, ft	KCAS, nmi/h	Mach number	Altitude, ft	Dynamic pressure, lbf/ft^2	KCAS, nmi/h	Static pressure, psia	TC 1, °F	TC 2, °F
1	0.71	20,012	330.0	0.70	20,007	337.5	329.7	6.8	55.2	53.1
	0.71	20,021	329.8	0.70	20,032	337.5	329.8	6.7	52.0	51.3
	0.72	20,020	332.0	0.71	20,050	341.2	332.2	6.7	51.1	49.5
	0.72	10,240	398.0	0.71	10,432	509.7	401.4	9.9	86.8	89.4
	0.71	10,245	396.3	0.71	10,422	505.2	399.1	9.9	85.9	84.0
	0.72	10,243	398.7	0.71	10,436	510.3	401.7	9.9	87.7	89.4
2	0.71	10,224	396.8	0.71	10,395	506.5	399.7	10.0	88.1	86.5
	0.72	10,215	399.9	0.72	10,405	512.8	402.9	9.9	88.1	85.6
	0.71	10,223	397.2	0.71	10,407	507.1	400.0	9.9	87.2	83.8
	0.61	7,749	350.9	0.61	7,940	406.3	354.9	10.9	79.6	78.2
	0.61	7,741	352.7	0.61	7,950	410.4	357.0	10.9	79.6	78.7
	0.60	7,698	347.2	0.60	7,818	396.8	349.7	11.0	79.2	76.9
3	1.22	28,483	501.7	1.23	28,926	700.6	506.0	4.6	63.9	58.8
	1.22	28,471	502.8	1.23	28,832	701.9	506.4	4.6	62.6	62.0
	1.21	28,469	500.6	1.23	28,932	698.6	505.4	4.6	63.9	62.5
	1.21	28,469	496.6	1.22	28,986	687.2	501.7	4.6	68.4	66.7
	1.21	28,467	499.2	1.22	28,898	692.6	503.4	4.6	69.3	67.6
	1.21	28,470	496.4	1.22	28,963	684.6	500.8	4.6	69.3	67.6
4	1.57	38,293	536.6	1.63	40,206	722.9	552.9	2.7	108.1	110.6
	1.57	38,286	536.5	1.63	40,201	722.8	552.8	2.7	108.9	114.2
	1.57	38,287	535.9	1.63	40,258	721.4	552.5	2.7	109.8	114.2
	1.57	38,290	536.3	1.63	40,228	722.0	552.6	2.7	112.9	114.0
	1.57	38,295	535.7	1.63	40,291	720.1	552.1	2.7	112.0	111.8
	1.57	38,300	536.3	1.63	40,226	721.7	552.5	2.7	111.1	108.7

Table 1. Continued.

Divot ejection conditions					Results		
Divot	Tank pressure, psia	Tank temp., °F	Line pressure, psia	Line temp., °F	Divot ejection	Divot stability	Comments
A	296.1	57.0	69.0	62.9	OK	NA	
B	287.0	60.2	62.7	54.8	OK	NA	
C	280.9	49.2	62.7	52.9	OK	NA	
G	273.7	54.7	64.4	53.4	OK	NA	
H	268.4	44.2	65.0	52.0	No divot ejection	NA	
I	263.8	56.5	65.9	56.6	OK	NA	
A	296.9	53.3	76.7	64.7	OK	Trim	
B	285.2	66.0	68.2	69.2	OK	Trim	
C	277.7	56.5	68.2	70.1	OK	Trim	Very small foam piece flaked off at ejection.
G	265.2	69.6	70.0	71.9	OK	No Trim	Divot may have tumbled after first full oscillation.
I	258.8	69.6	70.0	71.9	OK	No Trim	Divot tumbled after first full oscillation.
H	248.1	70.1	70.0	71.9	No divot ejection	NA	
H	296.1	44.2	77.8	53.4	OK	Trim	
G	288.4	56.5	67.1	54.8	OK	Trim	
I	281.2	55.2	67.0	54.8	OK	Trim	
A	272.6	55.2	67.6	54.8	OK	Trim	
B	268.4	55.2	67.5	53.8	OK	Trim	
C	260.6	55.2	67.1	54.8	OK	Trim	Very small foam piece flaked off at ejection.
H	299.0	47.0	75.1	49.7	OK	Trim	
G	291.3	54.3	62.8	50.2	OK	Trim	
I	285.2	54.3	62.7	50.2	OK	Trim	
A	277.4	53.3	62.7	49.7	OK	Trim	
B	269.4	54.3	62.8	50.2	OK	Trim	
C	263.8	54.3	63.4	50.2	OK	Trim	

Table 1. Continued.

Flight No.	Aircraft flight conditions			AFTF flight conditions					Foam temperature	
	Mach number	Altitude, ft	KCAS, nmi/h	Mach number	Altitude, ft	Dynamic pressure, lbf/ft^2	KCAS, nmi/h	Static pressure, psia	TC 1, °F	TC 2, °F
5	1.74	45,866	508.0	1.79	47,722	605.5	533.4	1.9	138.4	144.0
	1.75	45,803	509.8	1.79	47,599	610.7	535.7	1.9	138.4	145.3
	1.75	45,725	511.7	1.79	47,332	616.8	537.7	1.9	138.8	145.7
	1.76	45,650	513.8	1.79	47,213	622.4	540.1	1.9	142.8	143.0
	1.76	45,581	515.7	1.79	47,030	628.2	542.3	1.9	143.6	142.1
	1.77	45,516	518.2	1.80	47,018	634.9	545.9	1.9	144.5	143.0
6	1.20	27,108	506.4	1.20	27,358	710.7	508.6	4.9	90.7	76.5
	1.21	27,118	510.2	1.22	27,699	729.5	514.9	4.8	92.1	79.1
	1.20	27,120	509.5	1.22	27,743	728.1	514.5	4.8	91.6	78.3
7	1.19	27,051	505.0	1.19	27,278	707.2	507.3	4.9	64.8	60.2
	1.20	27,063	506.8	1.20	27,339	713.0	509.4	4.9	63.9	63.8
	1.20	27,065	508.8	1.21	27,428	721.4	512.2	4.9	65.2	63.8
8	1.20	27,165	508.1	1.22	27,786	723.8	513.1	4.8	78.2	74.7
	1.20	27,168	508.4	1.22	27,768	724.5	513.4	4.8	78.2	76.5
	1.20	27,173	508.6	1.22	27,761	724.8	513.5	4.8	78.2	77.4
9	1.97	47,191	554.9	1.99	48,243	730.4	611.9	1.8	152.4	164.6
	1.97	47,257	555.9	1.99	48,242	734.1	613.9	1.8	152.4	164.6
	1.98	47,299	556.7	2.00	48,354	735.5	615.8	1.8	153.3	165.9

Table 1. Continued.

Divot ejection conditions					Results		
Divot	Tank pressure, psia	Tank temp., °F	Line pressure, psia	Line temp., °F	Divot ejection	Divot stability	Comments
H	295.0	50.6	77.6	46.5	OK	Trim	
G	287.6	50.6	61.8	46.5	OK	Trim	
I	281.2	51.1	61.8	47.5	OK	Trim	
A	274.8	51.5	62.3	46.5	OK	Trim	
B	267.6	51.5	61.8	47.5	OK	Trim	
C	260.9	51.1	62.2	46.5	OK	Trim	
D	292.6	64.2	33.0	64.7	No divot ejection	NA	
E	292.9	69.2	24.3	67.4	No divot ejection	NA	
F	292.9	67.8	19.9	66.5	No divot ejection	NA	
D	294.7	60.2	49.5	61.1	Partial divot ejection	NA	Divot recontacted with parent hole and broke upon recontact. Large portion of divot appeared to remain in hole. Leading and trailing edges broke off and traveled downstream.
E	290.5	60.6	39.9	61.1	OK	Trim	
F	287.6	60.6	40.5	61.1	Partial divot ejection	NA	Same as divot D. More of the divot appeared to break free and travel downstream. Some of the debris recontacted the partial divot D and shattered. Difficult to determine whether or not the pieces trimmed.
D	301.4	61.1	62.6	63.8	OK	Trim	
E	295.0	64.2	54.3	62.0	OK	Trim	
F	290.5	64.2	54.2	62.9	OK	Trim	
D	299.3	49.7	59.1	49.7	OK	Trim	
E	292.9	53.3	50.6	49.7	OK	Trim	
F	287.0	51.1	50.3	49.7	OK	Trim	

Table 1. Continued.

Flight No.	Aircraft flight conditions			AFTF flight conditions					Foam temperature	
	Mach number	Altitude, ft	KCAS, nmi/h	Mach number	Altitude, ft	Dynamic pressure, lbf/ft^2	KCAS, nmi/h	Static pressure, psia	TC 1, °F	TC 2, °F
10	1.53	34,026	569.4	1.60	36,186	841.2	585.5	3.3	107.2	108.0
	1.53	34,021	569.5	1.60	36,195	841.7	585.7	3.3	107.2	108.9
	1.53	34,011	569.8	1.60	36,174	843.0	586.1	3.3	106.7	110.2
	1.53	34,002	570.3	1.60	36,201	844.2	586.5	3.3	108.5	108.7
	1.53	33,992	571.1	1.60	36,086	845.7	586.8	3.3	107.6	107.8
	1.53	33,989	571.7	1.60	36,124	848.1	587.7	3.3	106.7	106.9

Table 1. Concluded.

Divot ejection conditions						Results	
Divot	Tank pressure, psia	Tank temp., °F	Line pressure, psia	Line temp., °F	Divot ejection	Divot stability	Comments
H	317.9	63.8	73.5	61.1	OK	Trim	
G	309.9	65.6	64.3	62.0	OK	Trim	
I	303.5	64.2	64.4	61.1	OK	Trim	
A	293.9	65.6	64.3	62.0	OK	Trim	
B	289.7	65.6	65.0	62.0	OK	Trim	
C	282.8	65.6	64.4	62.0	OK	Trim	Passed through the first oscillation before trimming with large diameter forward.

High-Speed Digital Video Camera System

Two flight-qualified, high-speed camera systems were required to achieve the experiment objectives. The camera systems were synchronized with the divot ejection system, which was simultaneously triggered by an aft cockpit switch to capture the images and record them on a solid-state recorder within the camera systems. The two camera systems and data acquisition systems were correlated with the onboard GPS-synchronized, IRIG-B time. The high-speed digital camera system was comprised of the following components: camera controller and recorder units, camera heads, synchronization and divot ejection system interface relay circuitry, and M-Hub junction box (fig. 5).

The camera controller and recorder units were located in the ammunition bay pallet accessible from underneath the aircraft, forward of the AFTF leading edge. The synchronization card and relay cards were located in the upper aft instrumentation bay of the AFTF. To survive in the flight environment, this equipment was shock mounted on vibration isolators.

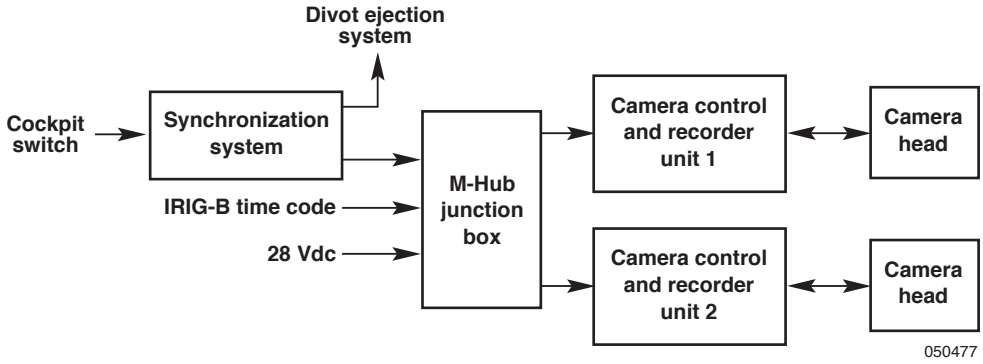

Figure 5. High-speed camera system components and interfaces.

For all of the flight tests, the camera configuration was set at a frame rate of 2,000 pps, exposure rate of 50 microseconds, resolution of 1280 by 512 pixels ranged over the field of view, and software gain of +6 dB. The camera system had the capability to record at a maximum frame rate of 10,000 pps; however, operating at this rate reduced the record time and resolution. Each camera had a cumulative video recording capacity of 9.6 seconds. Based on extensive ground testing, this camera configuration provided optimum conditions for capturing the divot ejection video. The high-speed video captured images of the divot release and to approximately 5 ft (1.524 m) downstream of the release point. The focal lengths of the forward and aft camera lenses were 25 and 11.6 mm, respectively. Only in-flight ambient lighting was used for all video recordings.

Divot Photogrammetry and Trajectories

Standard photogrammetry analysis techniques, which use photographic images to obtain measurements of position, were used to estimate the divot trajectories from the high-speed digital video. The divot spatial position, rotation, and velocity were estimated for the in-flight ejections.

Multiple reference points on the divot were used to determine rotation. Velocity was calculated by differentiating the spatial coordinates with respect to time. Reference 7 provides details and results of the photogrammetry technique.

Camera Pods

The high-speed camera heads were housed in camera pods mounted on the forward and aft fuselage left side missile rail stations (fig. 2). The camera pods are made of aluminum and have a wedge shape. The forward camera pod has a length of 46 in. (1.17 m) and a leading-edge wedge angle of 13.4°. The aft camera pod has a length of 50.8 in. (1.29 m) and a leading-edge wedge angle of 13.88°. Each camera pod has a removable 1/4-in-thick (6.35 mm), borosilicate crown optical glass window with an antireflective coating.

The forward camera had a field of view of approximately 34° and a view width of approximately 5 ft (1.524 m) at an object distance of roughly 10 ft (3.048 m). The aft camera had a field of view of approximately 67° and a view width of approximately 5 ft (1.524 m) at an object distance of roughly 4 ft (1.22 m). The camera head mount in the camera pod permitted fine adjustment of the viewing area of approximately –2° to +7° up and down and ±10° left to right. Figure 6 shows the forward and aft camera viewing angles relative to the AFTF.

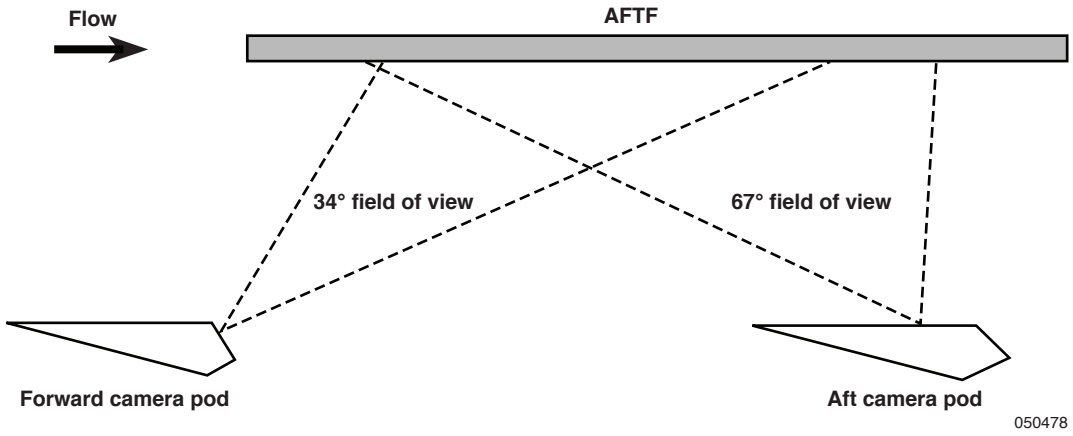

Figure 6. Camera pod views relative to the Aerodynamic Flight Text Fixture.

Several factors were considered in the aerodynamic design of the camera pods. The right inboard side of each camera pod was parallel to the free-stream flow to reduce shock wave impingement on the AFTF. The camera pod leading-edge turning angle was on the left outboard side of each pod. The forward camera pod leading-edge wedge angle was selected to ensure an attached shock wave at Mach 1.6 and greater.

For structural design considerations, aerodynamic analyses were conducted on the camera pods to assess leading-edge shock wave locations, base region reattachment shock locations, base region wake flow impingement, and pressure distributions. Analyses included application of

simple shock-expansion wave theory and three-dimensional (3-D), inviscid computational fluid dynamics (CFD).

The 3-D CFD was for the complete F-15B aircraft with the AFTF and camera pods attached. The CFD calculations were made for the Mach 1.2, 1.6, and 2.0 supersonic flight test conditions. Figure 7 shows the results for the Mach 2 case. For all of the supersonic CFD cases, no indication of shock impingement on the AFTF was observed from the camera pods.

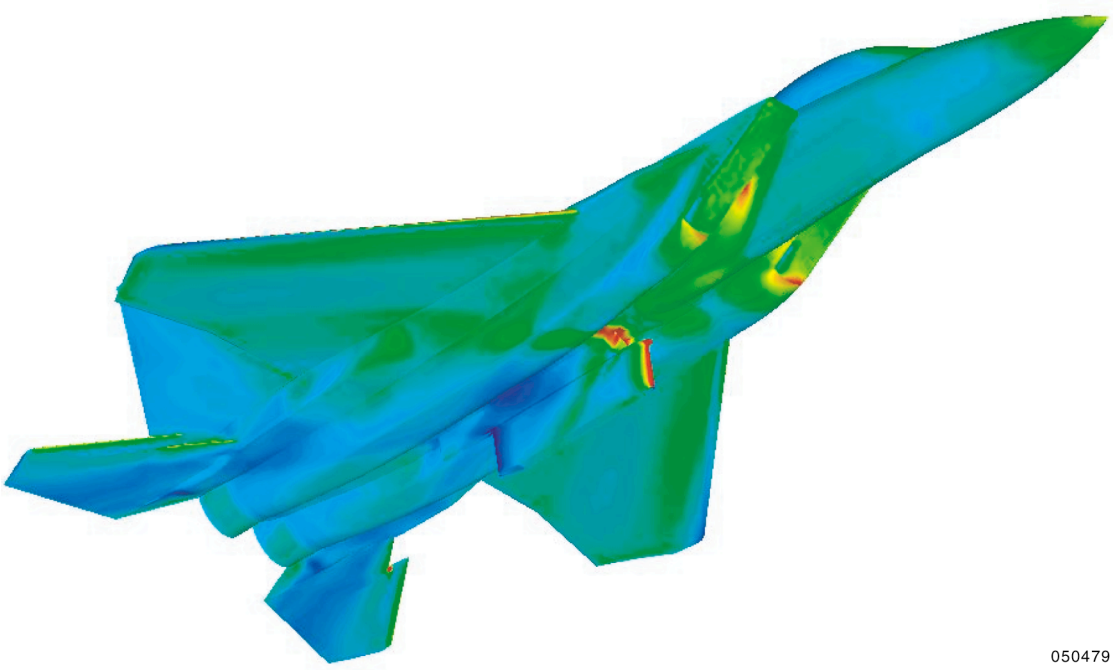

(a) Complete aircraft.

Figure 7. The F-15B aircraft computational fluid dynamics analysis.

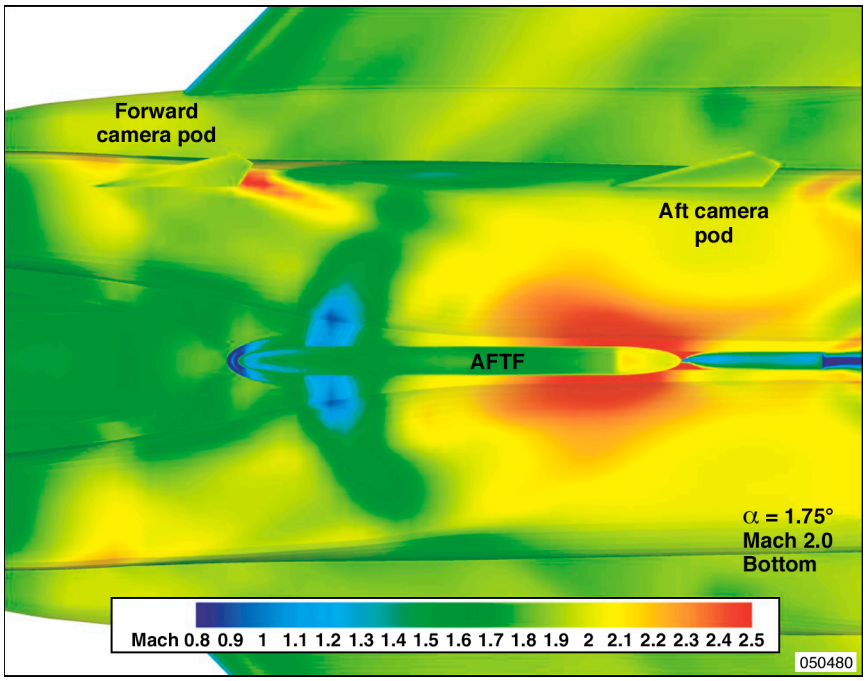

(b) Bottom of aircraft.

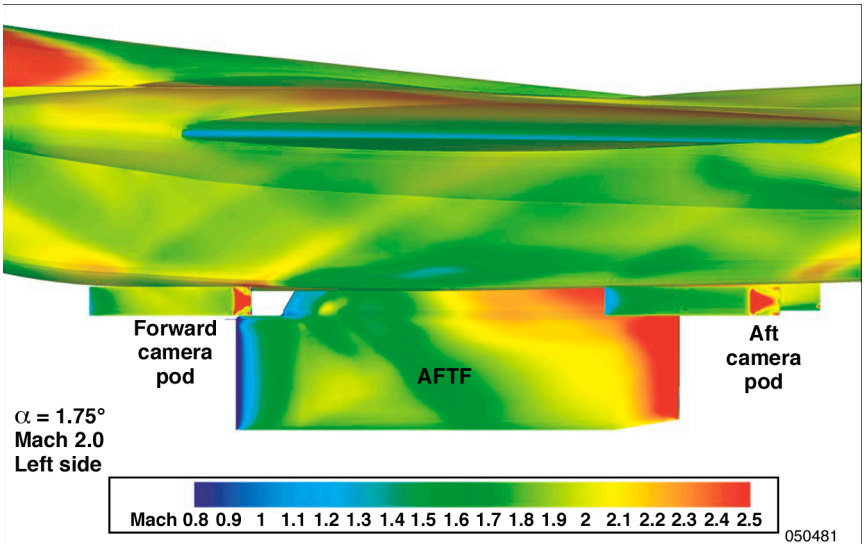

(c) Left side of aircraft.

Figure 7. Concluded.

The impact of the camera pods on aircraft stability and control was predicted based on comparison to other stores. The main area of concern was degradation in the lateral-directional stability of the F-15B aircraft at high supersonic speeds. During a previous flight experiment, a longer camera pod with a shortened span had been successfully carried on the F-15B missile rail stations. This pod was flown to Mach 2 with no stability and control issues. The size of the present camera pods also was compared to that of the AIM-7 Sparrow air-to-air missile (Raytheon Company, Waltham, Massachusetts, and General Dynamics Propulsion, now Aerojet-General Corporation, Rancho Cordova, California). Two AIM-7 Sparrow missiles can be carried simultaneously on the F-15B forward and aft missile rails and carriage of the missiles is cleared for the full F-15B flight envelope. The side force area for the two camera pods, which impact lateral-directional stability, was approximately 60-percent less than the area for the two AIM-7 Sparrow missiles. No stability and control issues were anticipated based on the significantly smaller side force area, and none were encountered in flight.

Static and dynamic structural analyses were performed to verify the structural integrity of the camera pods. The camera pods had positive static structural margins of safety, with a 2.25 factor of safety, for the worst-case pressure loads at 600 kn (308.7 m/s), sea level altitude.

An aluminum conduit, 0.75 in. (0.1905 m) in diameter and approximately 12 ft (3.66 m) long, was externally mounted from the aft end of the forward missile rail to the forward end of the aft missile rail to house the camera system video cable. Simple band clamps and 12 fasteners were used to attach the external conduit to the aircraft fuselage. A MIL-S-8802 fuel tank sealant-adhesive was used to fair the sides of the conduit into the fuselage. Aerodynamic pressure and skin friction loads were calculated for the external conduit to ensure that the fastener arrangement was adequate.

Foam Sheets

The foam sheets were constructed out of aluminum plates that had been sprayed with shuttle external tank Stepanfoam® BX-265 (Stepan Company, Northfield, Illinois) TPS insulating foam. The foam thickness was 2 in. (0.0508 m). Three AFTF bays were configured to carry a foam sheet, bays 2B, 3A, and 3B (fig. 4). Six foam sheets were sprayed for each AFTF bay. One sheet from each bay was used for ground testing and the remaining five from each bay were used for flight testing.

In addition to the Stepanfoam BX-265 foam, an inexpensive closed-cell blue Styrofoam® (Dow Chemical Company, Midland, Michigan) was used for the ground test and early flight test. The Styrofoam has a density of 2.0 lbm/ft^3 (32.0 kg/m^3), similar to the density of the Stepanfoam BX-265 foam. The Styrofoam was an easily available, inexpensive substitute for the actual shuttle foam for development of the divot ejection system and functional checkouts. The Stepanfoam BX-265 foam was sprayed on, whereas the blue Styrofoam was simply cut to the desired dimensions and bonded onto the aluminum backing plates with a MIL-S-8802 adhesive. Despite the difference in the way in which the foam was attached to the backing plates, the divots produced from the blue Styrofoam were very similar to those produced from the Stepanfoam BX-265 foam.

Cylindrical voids were precut into the back of the foam sheets adjacent to the aluminum plate, simulating an air void on the shuttle external tank. Nitrogen gas was used to pressurize the void through a hole in the aluminum plate. The foam next to the void was scored to assist in creating a fracture line when the foam was back pressured. Each sheet had three voids and therefore was capable of producing three divots.

Figure 8 and table 2 show the foam plate dimensions and divot sizes, respectively, including the void diameters and depths. The divot sizes used in the flight test were selected based on predictions for the largest expected voids at various locations on the shuttle external tank. The void diameter varied from 0.31 to 1.68 in. (0.007874 to 0.017272 m). The void depth varied from 0.89 to 1.35 in. (0.02261 to 0.03429 m). The predicted divot diameter produced from these void sizes varied from 2.5 to 5.5 in. (0.0635 to 0.1397 m). Foil thermocouples were used to measure foam surface temperatures at two locations on each foam sheet. The thermocouples were bonded to the sheet near the corner edges of the panels so as not to aerodynamically interfere with the divot ejection.

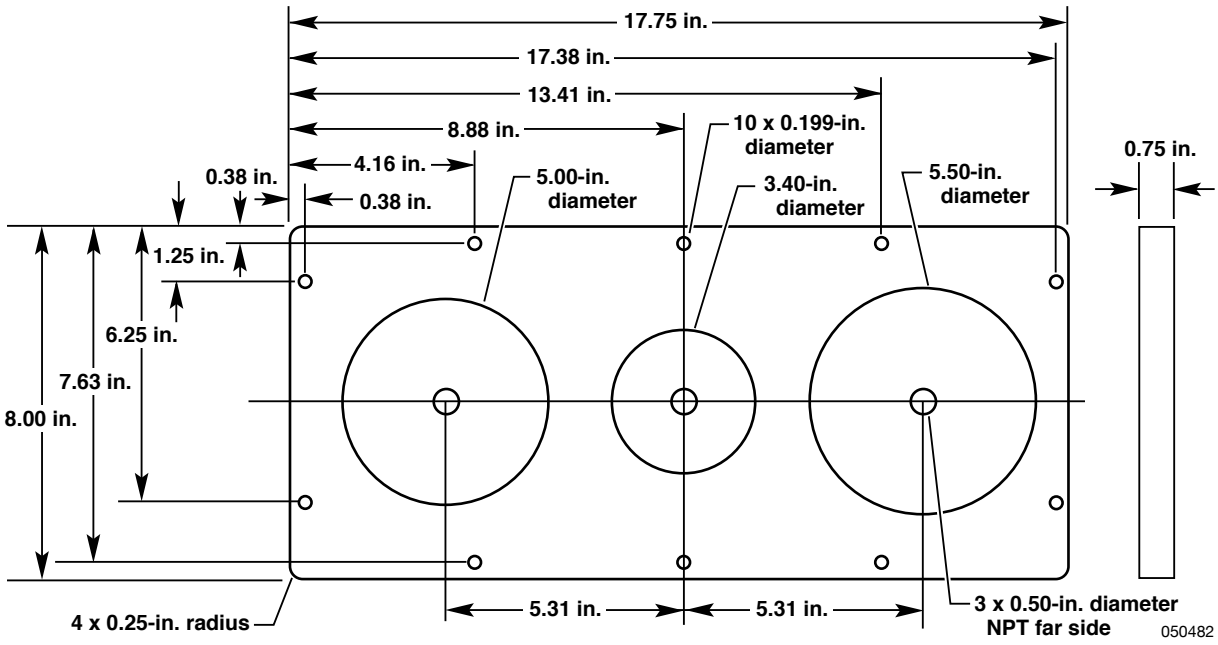

(a) Bay 2B foam sheet.

Figure 8. Aerodynamic Flight Test Fixture foam plate dimensions and divot sizes.

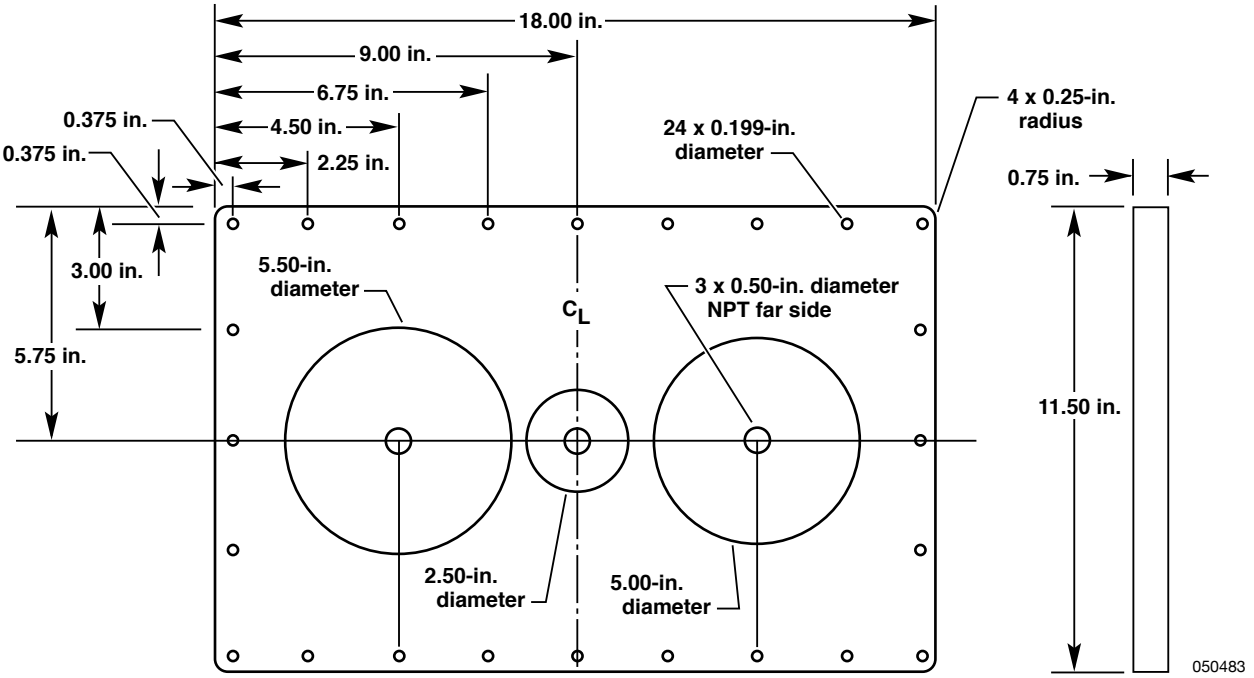

(b) Bay 3A foam sheet.

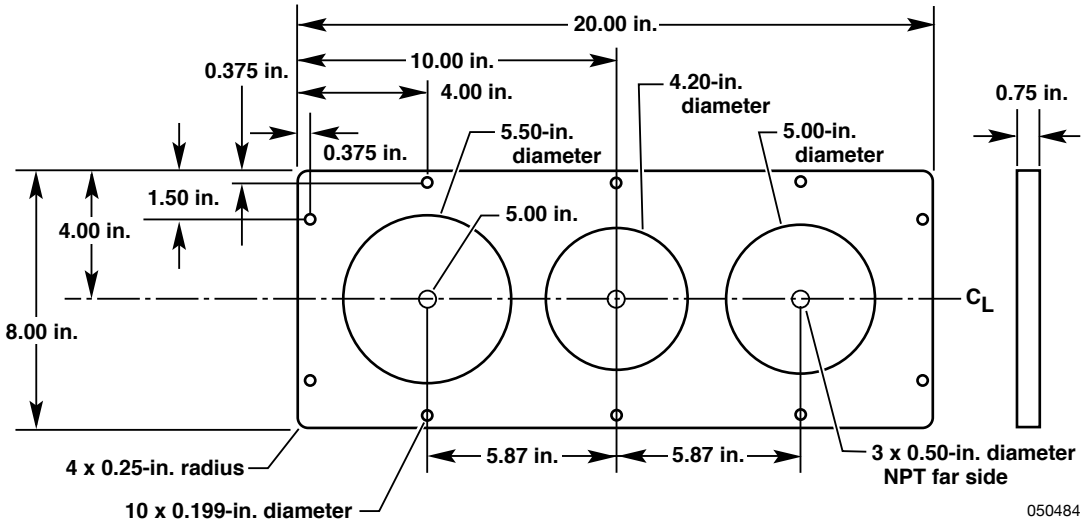

(c) Bay 3B foam sheet.

Figure 8. Concluded.

Table 2. Divot cases.

Case	Void diameter, in.	Void depth, in.
1	0.31	1.35
3	1.30	1.00
5	0.56	1.17
7	1.67	0.89
9	1.68	1.05

Divot Ejection System

The pressure required to eject divots from the foam sheets was supplied by a pneumatic system carried in the aft section of the AFTF. Major components of the pneumatic system included a reservoir tank, manual fill valve, manual final stop valve, pressure regulator, electric solenoid valves, and associated fluid lines. Figure 9 illustrates the pneumatic system, and table 3 provides details of the pneumatic system components. Pneumatic system measurements included tank pressure, tank wall temperature, regulated pressure, and gas temperature downstream of the pressure regulator.

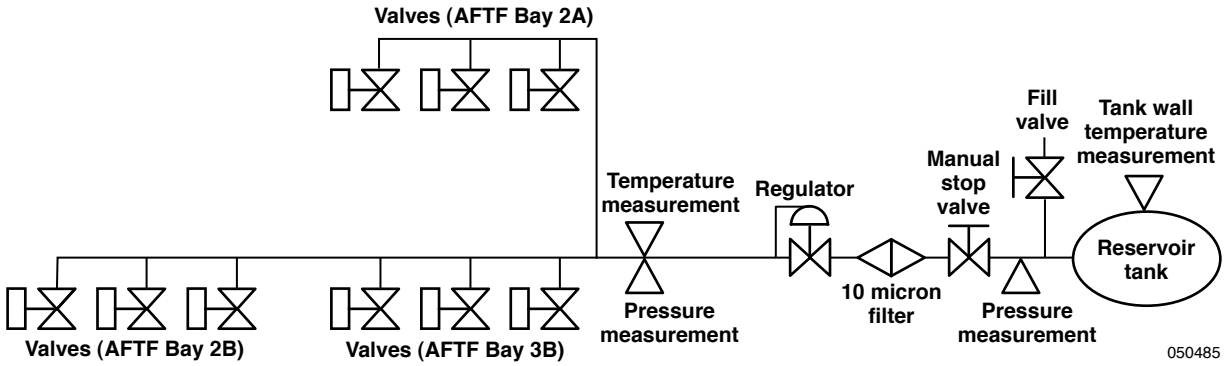

Figure 9. Divot ejection pneumatic system.

Table 3. Divot ejection pneumatic system components.

Component	Manufacturer	Model / part No.	MEOP, lbf/in^2	Burst pressure, lbf/in^2	Operating temperature, °F
Tank (200 in^3)	Lockheed Martin Corporation, (Bethesda, Maryland)	Type 30-40, MIL-R-8573A(ASG)	3,000	6,650	–65 to +325
Fill needle valve	Alta-Robbins (Lindon, Utah)	SSKG250-4T	6,000	24,000	–40 to +250
Manual stop ball valve	Swagelok Company (Solon, Ohio)	SS-43TS4	3,000	NA	–65 to +150
Regulator	Swagelok Company	SS-HFML3B-VCR4-P-BK	500	NA	–10 to +150
Solenoid valve	Marotta Controls, Inc. (Montville, New Jersey)	MV510H/ 805764-3312	6,000	18,000	–65 to +165
Fluid lines	NA	6061T6 aluminum	1,500	6,000	NA
Filter	Wintec Industries (Fremont, California)	12267-556	3,000	NA	–423 to +800

The pneumatic system complied with MIL-STD-1552A, "General Requirements for Safe Design and Operation of Pressurized Systems" (ref. 8). No relief valves were required in the system, because the maximum expected operating pressure (MEOP) could not be exceeded by design.

The 200-cubic-in (0.00328 m^3) reservoir tank was filled with nitrogen gas to a nominal operating pressure of approximately 300 psia (2,068,427 N/m^2). The reservoir tank was connected to a pressure regulator that reduced the 300-psia source pressure to the required divot ejection pressure, nominally 40 to 80 psia (275,790 to 551,581 N/m^2). The regulator pressure was set to the desired ejection pressure on the ground before flight. The regulator was plumbed to solenoid valves that were attached to the backs of the foam sheets. The solenoid valve was opened for 300 milliseconds, which back pressured the foam sheet, resulting in a divot ejection.

Synchronization System

A system was developed to synchronize the high-speed camera and divot ejection systems. The synchronization system digital card triggered the high-speed camera and the divot ejection in a timed and sequential order. A relay card was developed to provide the switching interface between the digital card and divot ejection system. The synchronization system instrumentation included monitoring of the digital card trigger impulses.

Two types of divot ejection triggering actions were possible, a single-mode trigger and a multiple-mode trigger. The single trigger option provided a single divot ejection and video recording for each individual trigger action. This option provided the flexibility to eject single divots at

various test conditions during the same flight or to simply allow time between divot ejections. The multiple trigger option, which was used for the supersonic test points, ejected multiple divots, with a preset 3-second delay between ejections. The 3-second delay between firings allowed the volume of gas between the regulator and solenoid valves to recover to the set regulator pressure.

The digital logic card used a programmable logic device to provide the desired sequencing, delays, and holds. The trigger pulse time duration for activation of the divot ejection system solenoid valves was 300 milliseconds. This value was set by counters that were compared to a reference number. The trigger pulse time duration then could be easily changed by simply changing the reference number in the synchronization software code. The relay card operated in conjunction with the digital card to drive the divot ejection system solenoid valves.

The control panel that included the trigger function was located in the F-15B aft cockpit and contained the following switches: initiate, mode, arm, and trigger (fig. 10). The initiate switch was a locking toggle switch that provided power to the digital card. The mode switch selected either the single or multiple trigger mode. The arm switch was a locking toggle switch that provided power to the relay interface card. A control panel lamp was illuminated when the arm mode was activated. The trigger switch was a guarded momentary switch that triggered the digital card to initiate the high-speed video and divot ejection sequence.

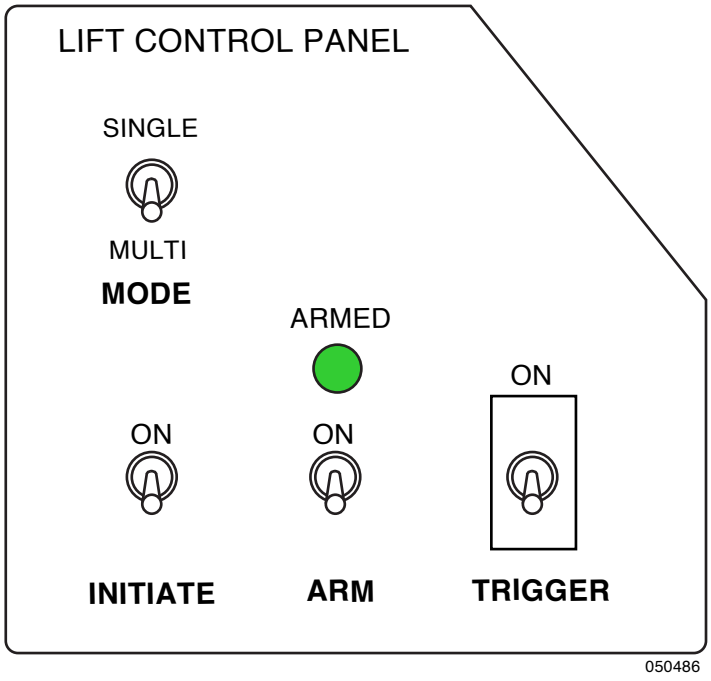

Figure 10. Lifting Insulating Foam Trajectory aft cockpit control panel.

Health monitoring outputs from the synchronization system were telemetered in real time to the control room. These outputs included the digital card “heartbeat” to verify initialization and correct function, camera record status, and arm switch status.

FLIGHT TEST CONDITIONS AND MANEUVERS

The flight envelope for the present flight test was bound by the operating limitations imposed by carriage of the AFTF (fig. 11). These limitations included an absolute speed limit of 600 kn (308.7 m/s), maximum Mach number of 2 because of heating of the AFTF composite structure, maximum dynamic pressure of 1,100 lbf/ft^2 (52,668 N/m^2), and a maximum value of the product of sideslip angle and dynamic pressure, βq, of 5,500 deg-lbf/ft^2 (263,341 deg-N/m^2). For aircrew safety, a maximum altitude of 50,000 ft (15,240 m) was imposed. All of the divot ejection flight test points were flown within the AFTF flight envelope.

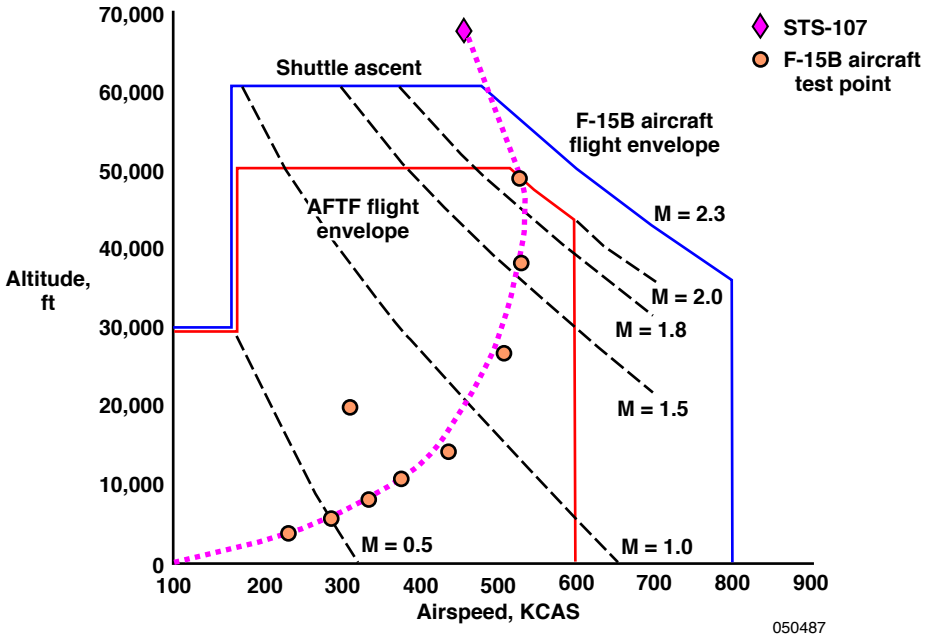

Figure 11. The F-15B aircraft Lifting Insulating Foam Trajectory flight test envelope and test points.

The flight test conditions included subsonic and supersonic test points to approximately Mach 2 and an altitude of 50,000 ft (15,240 m), which matched discrete points along the shuttle ascent trajectory (fig. 11). The test point at 330 knots calibrated airspeed (KCAS) (557 m/s), Mach 0.7, and an altitude of 20,000 ft is a "heart of the envelope" condition that was the first test point flown. Figure 12 compares the dynamic pressures from the LIFT test point and shuttle ascent. Because the local flow conditions measured at the AFTF differ slightly from the aircraft free-stream conditions, the aircraft flight condition was adjusted as required to match the AFTF local conditions with the desired shuttle ascent condition. The divot ejection was initiated at a flight test condition in which the wings were level, altitude was constant, and Mach number was constant. Table 1 presents the flight test points flown and the local flow conditions of both the aircraft and AFTF. For reference, the STS-107 mishap flight test condition was at Mach 2.5, an altitude of 69,000 ft (21,031 m), and a dynamic pressure of 425 lbf/ft^2 (20,349 N/m^2).

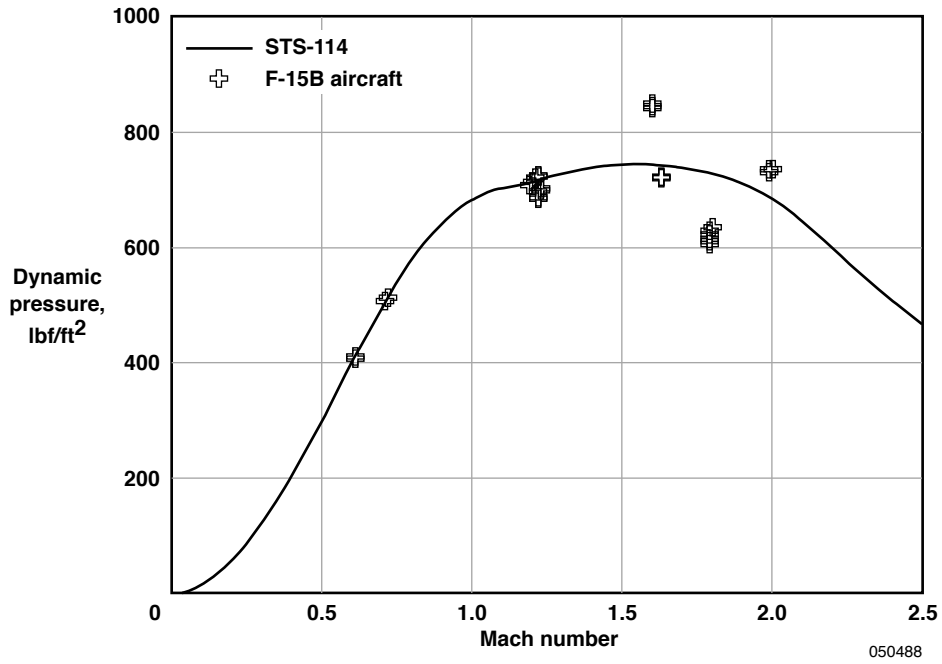

Figure 12. Comparison of dynamic pressures from the Lifting Insulating Foam Trajectory flight test point and shuttle ascent.

The divot ejection flight test conditions can be separated into three general categories: (1) maximum Mach number, (2) maximum dynamic pressure, and (3) maximum aerodynamic torque on the divot, embodied by the product of the divot moment coefficient and dynamic pressure, $C_m q$. The maximum Mach number test condition was at Mach 2.0, an altitude of 48,354 ft (14,738 m), and a dynamic pressure of 736 lbf/ft^2 (35,240 N/m^2). The maximum dynamic pressure test condition was at Mach 1.60, an altitude of 36,124 ft (11,011 m), and a dynamic pressure of 848 lbf/ft^2 (40,602 N/m^2). The maximum aerodynamic torque test condition was nominally at Mach 1.2, an altitude of 27,400 ft (8,352 m), and a dynamic pressure of 710 lbf/ft^2 (33,995 N/m^2).

HAZARDS ASSESSMENT

Two major hazards associated with the present flight test were the recontact of the ejected divot with the aircraft and divot ground impact issues. Assessment of the recontact hazard focused on the potential damage to the F-15B aircraft, whereas assessment of the ground impact hazard focused on the potential damage to property or injury to persons on the ground.

Divot Recontact

The divot recontact hazard was investigated from two approaches: predicting the trajectories of the ejected divots and evaluating the possible structural impact damage. Two techniques were used to

predict the divot trajectories: a simple one-degree-of-freedom (1-DOF) trajectory calculation and a simplified trajectory calculation through a 3-D CFD flow field.

The 1-DOF calculation modeled the divot as a point mass. The divot drag was specified as a function of Mach number only. The divot cross range was generated as a function of down-range distance by means of six-degree-of-freedom CFD models. The 1-DOF analysis predicted possible divot recontact with the aircraft with a lower probability of contact with the stabilizer. The prediction indicated no contact with the leading edge of the stabilizer.

The 3-D CFD analysis calculated the flow field around the complete F-15B aircraft with the AFTF attached. The divot trajectory then was computed as the divot moved through this steady 3-D flow field (fig. 13). The lift vector, moving the divot through the flow field, was calculated under the assumption of a worst-case alignment of the divot to produce the maximum lift. The 3-D flow fields about the AFTF were calculated for Mach 1.2, 1.6, and 2.0. The 3-D CFD analysis predicted some upwash in the aft region of the AFTF, downstream of divot release point. The predictions indicated that the foam divots could recontact the aft underside of the aircraft and stabilizers.

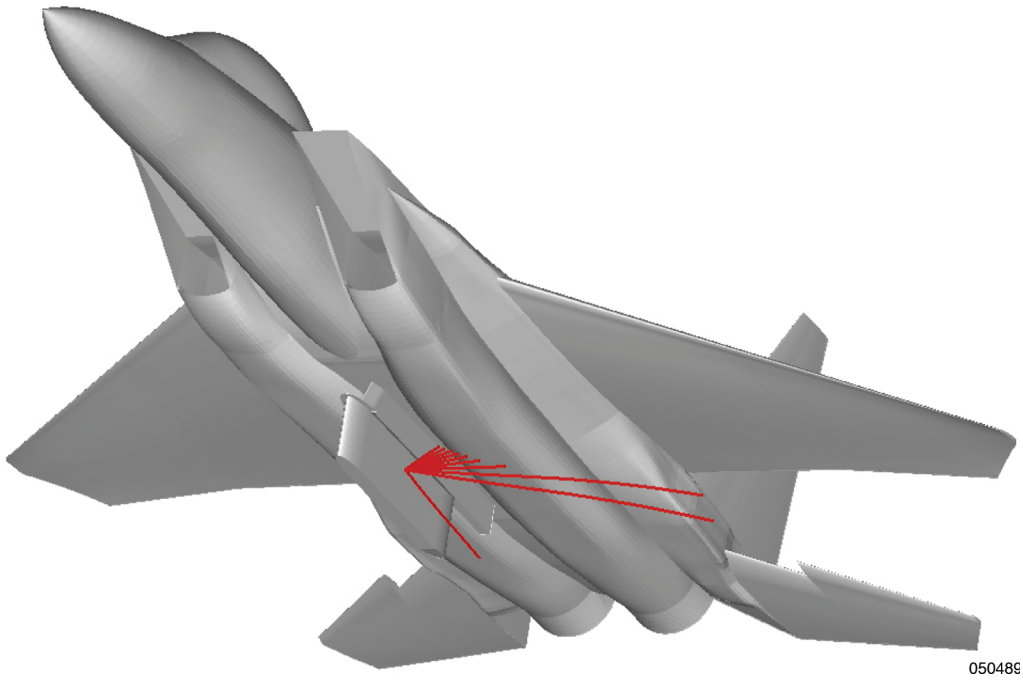

Figure 13. Divot recontact computational fluid dynamics predictions.

Because both trajectory analyses predicted that the divots could recontact the aircraft, a structural damage assessment was performed, based on a previous analysis by Ko (ref. 9) for another F-15 aircraft flight test in which shuttle foam was used. The first step in the damage assessment was to identify the structure and materials in the potential recontact area. These materials included various types of aluminum (2024-T81, 2024-T62, and 7075-T76) and titanium (6Al-4V). Two types of foam materials were assumed, shuttle external tank foam and blue Styrofoam. The

analysis was conducted assuming the worst case of a complete sheet of foam departing the AFTF and recontacting the aircraft.

The maximum strain energy density of the foam was compared to that of the aircraft structural materials (table 4). The maximum strain energy density of the shuttle foam is 0.65 in-lbf/in^3 (4,482 J/m^3), more than two orders of magnitude lower than the values for the aircraft materials. Based on this comparison, the foam was predicted to fail before the aircraft structure failed.

Table 4. Comparison of maximum strain energy density of foam and aircraft materials.

Material	Strain energy density, in-lbf/in^3
Foam	0.65
Aluminum (2024-T81)	166
Aluminum (7075-T76)	166
Aluminum (2024-T62)	105
Titanium (6Al-4V)	496

A 1-DOF trajectory analysis was used to predict the kinetic energy of the foam at a point 40 ft (12.2 m) downstream of the ejection point. This prediction provides a conservatively large value of the kinetic energy, because the distance from the divot ejection point to the trailing edge of the aircraft stabilizer is approximately 26 ft (7.92 m). The assumed dimensions of the foam sheet are 18 by 6.5 by 2 in. (0.4572 by 0.1651 by 0.1656 m). The kinetic energy of the foam sheet, 40 ft (1.016 m) downstream of the ejection point, is approximately 311 ft-lbf (421.7 J).

The energy required to compress the foam, E_{cr}, when a 90-percent void content is assumed, is 5,265 in-lbf (594.9 J) for the blue foam and 8,887 in-lbf (1,004 J) for the shuttle foam. Because the E_{cr} is much larger than the worst-case foam sheet kinetic energy, the foam is capable of absorbing the impact kinetic energy by compacting. This analysis is even further conservative, because it assumes that the foam hits the aircraft skin at an angle of 90° as opposed to an oblique impact.

The possibility of denting the aircraft skin also was evaluated. The aluminum honeycomb backing behind the aircraft skin has a yield stress between 14,000 and 37,000 lbf/in^2 (9.653x10^7 and 2.551x10^8 N/m^2). The stress induced by the honeycomb on the skin, resulting from the pressure force that the foam exerts on the skin from a foam impact, is 1,190 lbf/in^2 (56,978 N/m^2) for the blue foam and 2,009 lbf/in^2 (96,191 N/m^2) for the shuttle foam. Therefore, the possibility of denting the aircraft skin was predicted to be very small. Postflight visual inspections were performed and no damage from the divot impacts was found.

Divot Ground Impact

When the divot was ejected from the aircraft, the resulting ground impact possibly could have

posed a hazard to people or property, based on the kinetic energy of the divot or debris at ground impact. Based on the local test range predetermined criteria, ground safety was not an issue if the kinetic energy of the debris at impact was less than 11 ft-lbf (14.9 J). Two approaches were used to analyze this hazard: a simple analytical calculation of the divot kinetic energy based on its terminal velocity, and a more complex computation based on a 1-DOF trajectory simulation.

Equation 1 was used to calculate the divot impact kinetic energy, *KE*.

$$KE = \frac{1}{2}\frac{W}{g}V_{term}^2 \tag{1}$$

The kinetic energy was calculated under the assumption of the largest expected divot diameter, 7 in., resulting in a divot volume of 0.0223 ft^3 (0.000631 m^3) and a divot weight, *W*, of 0.0446 lb (0.02023 kg). Equation 2 was used to calculate the divot terminal velocity, V_{term}.

$$V_{term} = \sqrt{\frac{2W}{C_d \rho_{\text{air}} A_{cross-section}}} \tag{2}$$

The divot flat plate drag coefficient, C_d, was assumed to be 1.28 (ref. 10). A worst-case situation in which the divot falls from an altitude of 50,000 ft (15,240 m) was used with a conservative constant value of the air density, ρ_{air}, of 0.0003639 slugs/ft^3 (0.1877 kg/m^3). Two models of the divot cross-sectional area were used, the area assuming the divot falls "edge on" (7 in^2, 0.00452 m^2), and the area assuming the divot falls with its planform perpendicular to the flow (38.48 in^2, 0.02483 m^2).

When these assumptions are used, the terminal velocity and impact kinetic energy for the divot that falls edge on are 62.77 ft/s (19.13 m/s) and 2.73 ft-lbf (3.70 J), respectively. For the divot that falls with its planform perpendicular to the flow, the terminal velocity and impact kinetic energy are 26.77 ft/s (8.159 m/s) and 0.496 ft-lbf (0.672 J), respectively. The impact kinetic energy for both cases is well below the limit of 11 ft-lbf (14.9 J).

The 1-DOF computation is a higher fidelity prediction than the simple analytical calculation. It includes the proper variation of air density with altitude and an aerodynamic model that accounts for the tumbling of the foam piece. Two foam densities were considered, a "light" foam density of 1.8 lbm/ft^3 (28.8 kg/m^3), and a "heavy" foam density of 2.6 lbm/ft^3 (41.6 kg/m^3). The F-15B computation is a worst-case situation in which the entire foam sheet is assumed to depart the aircraft. The highest terminal velocity and kinetic energy obtained from the 1-DOF computations are 23 ft/s (7.01 m/s) and 3 ft-lbf (4.07 J), respectively.

Both types of calculations predicted ground impact kinetic energies well below the limit of 11 ft-lbf (14.9 J). Therefore, the divot ground impact hazard was not deemed a safety issue.

RESULTS AND DISCUSSION

A total of 10 divot ejection flights were completed, resulting in 41 successful, 5 failed, and 2 partial divot ejections. The blue Styrofoam was used in 5 of the successful divot ejections and 1 of the failed ejections. The shuttle foam was used in 36 successful, 4 failed, and 2 partial divot ejections. Table 1 provides a summary of the divot ejection flight conditions and results.

Flight Test Conditions

The flying qualities of the aircraft when the AFTF is attached are well known from the initial AFTF flight test program (ref. 3) and many subsequent flight tests in which the AFTF was attached. The new larger camera pods were not expected to cause any significant changes in the aircraft flying qualities. An envelope expansion process was followed to ensure that no adverse flying qualities were encountered, especially for high supersonic Mach numbers in which the F-15B lateral-directional stability decreases.

Table 1 presents the details of the aircraft and AFTF flight test conditions for all of the test points. Representative flight condition data are discussed for LIFT flight 9. The divot ejection flight test condition for this flight was nominally at Mach 2 and a pressure altitude of 48,250 ft (14,707 m), with a dynamic pressure of approximately 730 lbf/ft^2 (34,953 N/m^2). Three shuttle foam divots were successfully ejected at the Mach 2 test condition.

Figure 14 shows altitude as a function of Mach number for the acceleration from approximately Mach 0.9 to 2.0. Because of significant added drag from the AFTF and two camera pods, an optimum trajectory had to be followed to reach Mach 2. Figure 15 shows the specific excess power, P_s, overlaid on the altitude–Mach number plot. The P_s has been normalized by the maximum P_s value during the acceleration. The magnitude of the P_s is an indicator of the energy available to accelerate and/or climb.

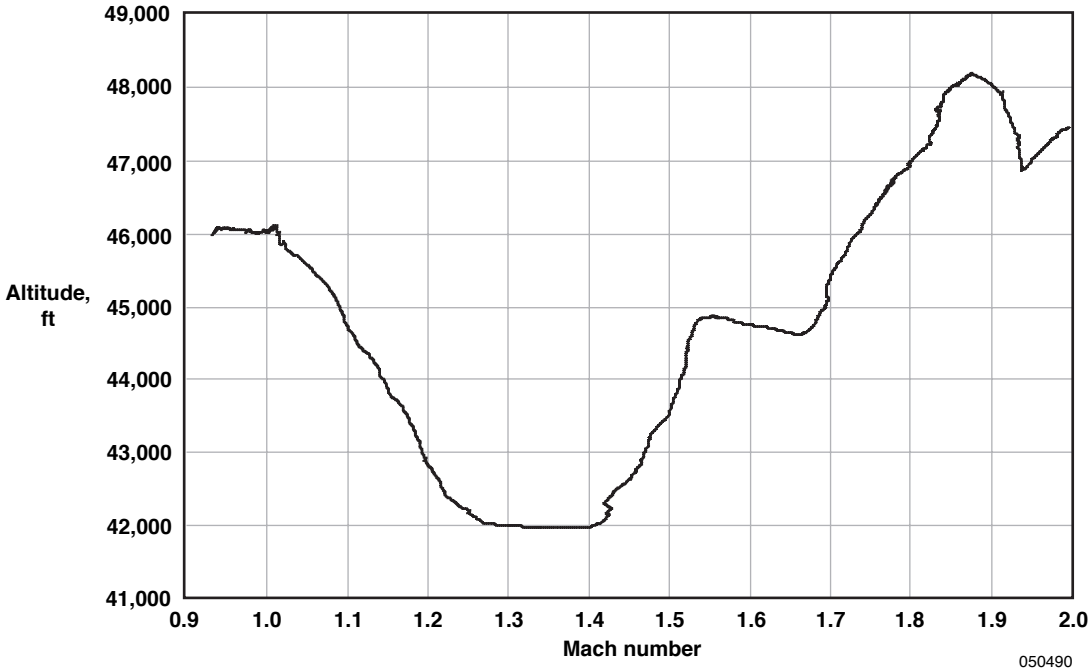

Figure 14. Altitude as a function of Mach number for supersonic acceleration (flight 9).

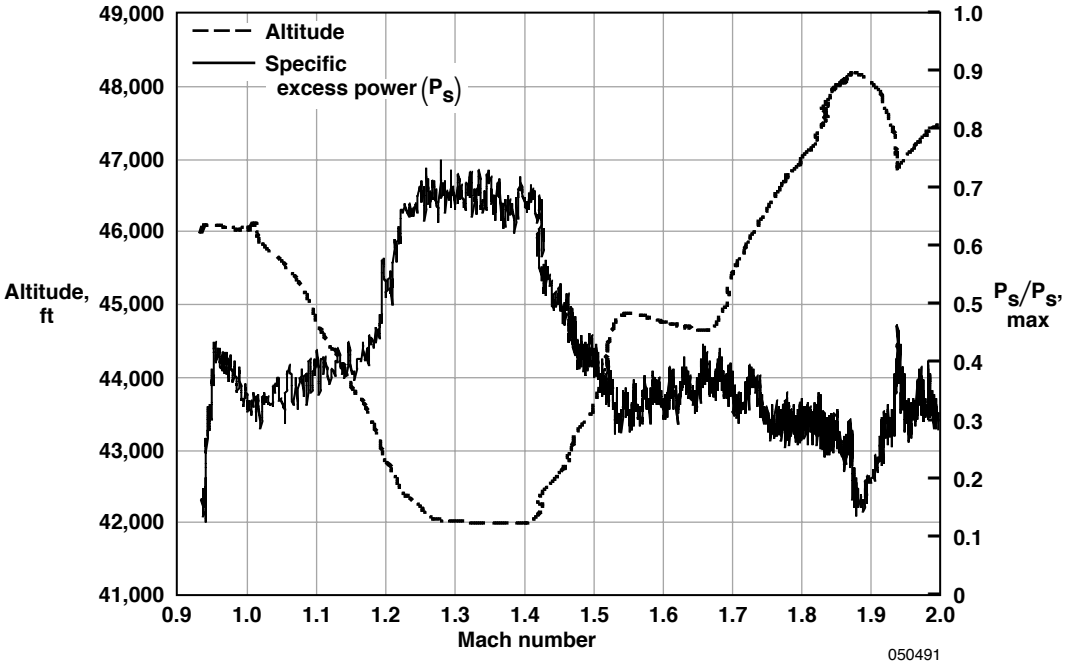

Figure 15. Specific excess power and altitude as a function of Mach number (flight 9).

In a region of lower P_s, the aircraft dove through to supersonic speeds from approximately Mach 0.9 at an altitude of 46,000 ft (14,021 m) to roughly Mach 1.27 at an altitude of 42,000 ft (12,802 m). At an altitude of approximately 42,000 ft (12,802 m), with a high value of P_s, the aircraft accelerated in level flight to roughly Mach 1.41. As the P_s decreased, the aircraft climbed to an altitude of approximately 45,000 ft (13,716 m).

Figures 16 and 17 show the aircraft angle of attack and angle of sideslip, respectively, as a function of Mach number. The angle of attack varied from a maximum of approximately 4.7° at roughly Mach 0.95 to a minimum of approximately 0.5° at Mach 2. The angle of sideslip was negative (nose right) below Mach 1.36 and slightly positive (nose left) above Mach 1.36. The angle of sideslip was approximately 0.2° at the Mach 2 test point.

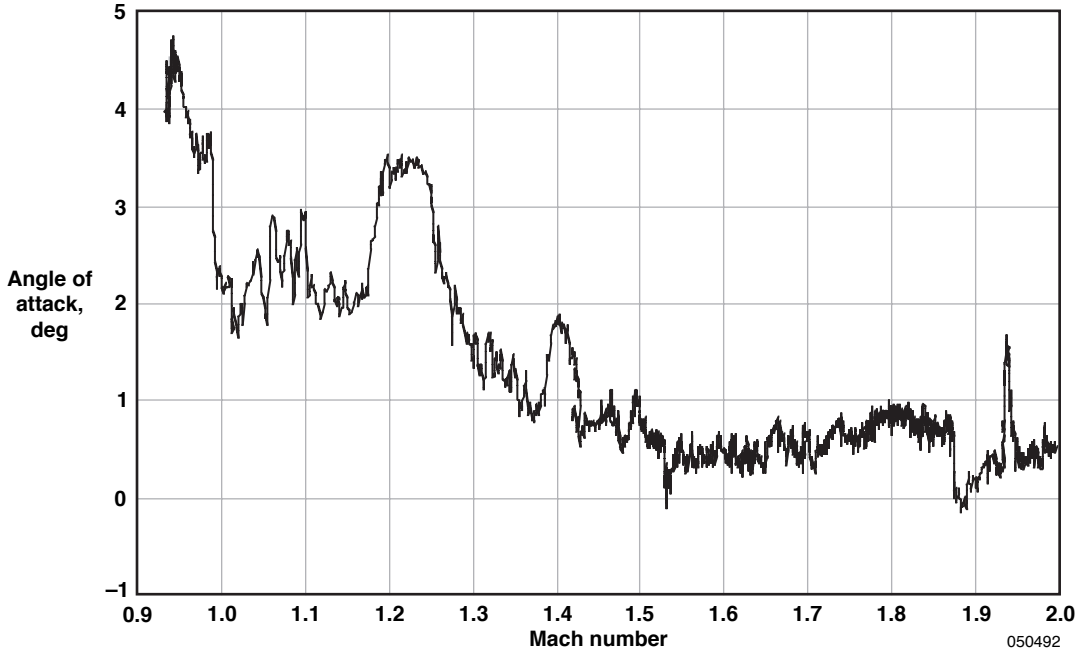

Figure 16. Angle of attack as a function of Mach number (flight 9).

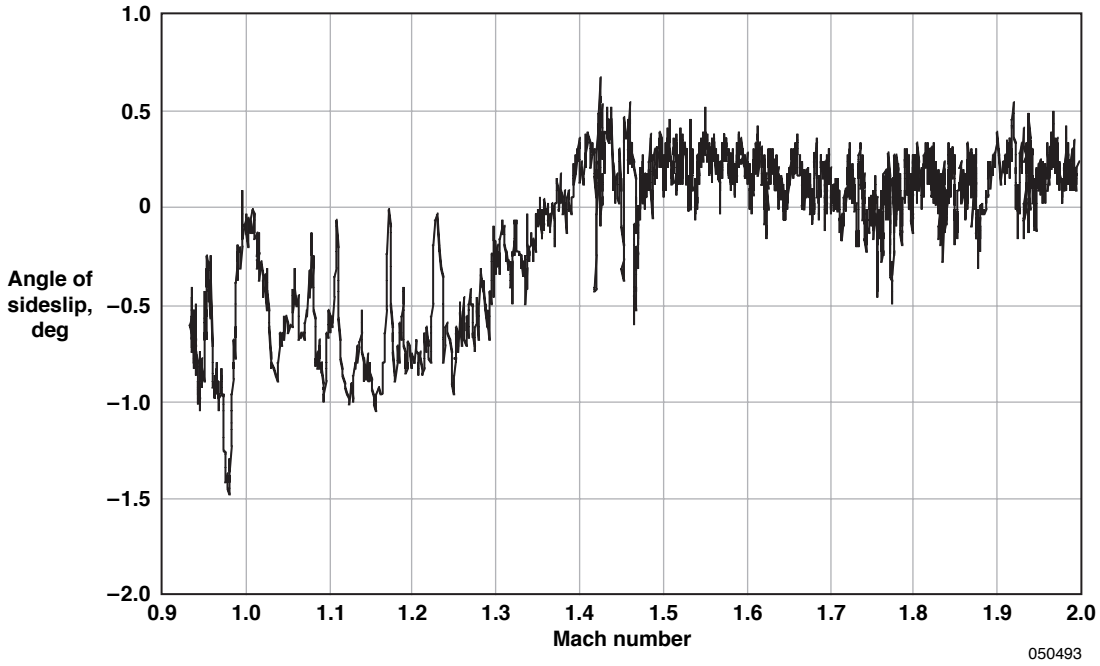

Figure 17. Angle of sideslip as a function of Mach number (flight 9).

Figure 18 compares the Mach numbers from the aircraft and the AFTF nose booms. Note that the AFTF local Mach number was different from the aircraft Mach number by as much as 0.1. Below approximately Mach 1.5, the AFTF measured Mach number was lower than the aircraft Mach number. At an aircraft Mach number between roughly 1.54 and 1.62, the AFTF Mach number was constant at approximately Mach 1.53, then increased discontinuously to match the aircraft value at roughly Mach 1.62. The lower AFTF Mach number in this region was caused by the passage of the aircraft inlet shock wave over the AFTF nose boom static pressure ports. When the Mach number of the aircraft was greater than approximately 1.7, the Mach number of the AFTF was greater than that of the aircraft, and the difference decreased to zero at roughly Mach 1.9.

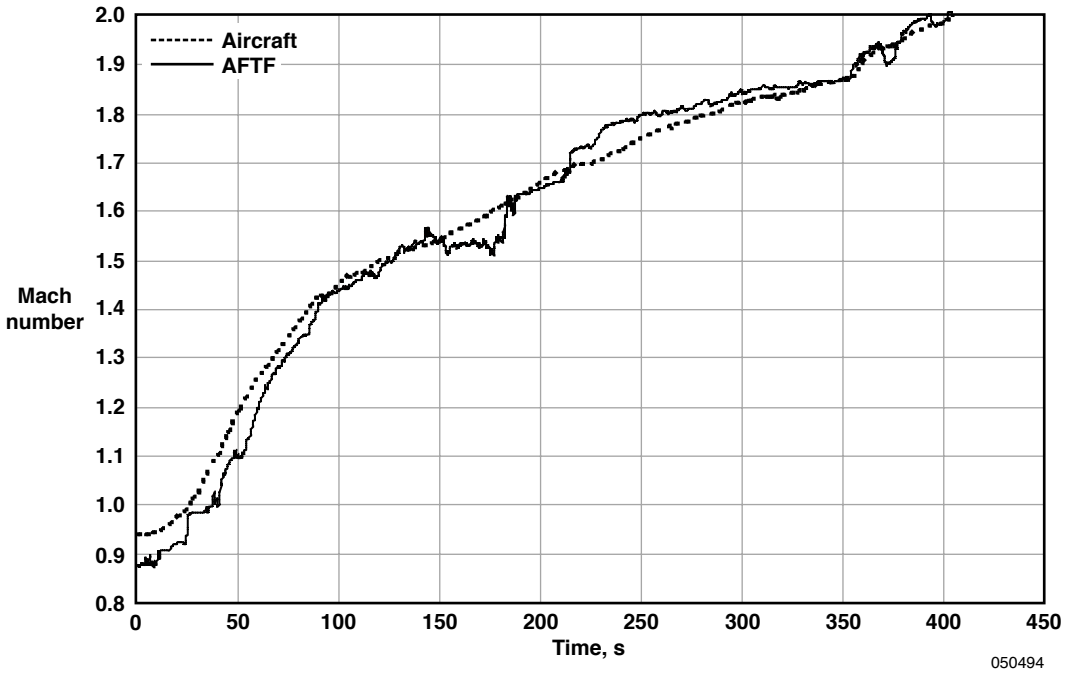

Figure 18. Comparison of Mach numbers from the aircraft and Aerodynamic Flight Test Fixture (flight 9).

Figure 19 compares the foam surface temperatures of the LIFT test points and shuttle trajectory as a function of Mach number. Recall that the F-15B aircraft test points were on the shuttle ascent trajectory, matching the Mach number and altitude, but the aircraft was not able to fly along the shuttle ascent trajectory to the test points. For this reason, the LIFT foam temperatures at the test points were lower than the shuttle foam temperatures.

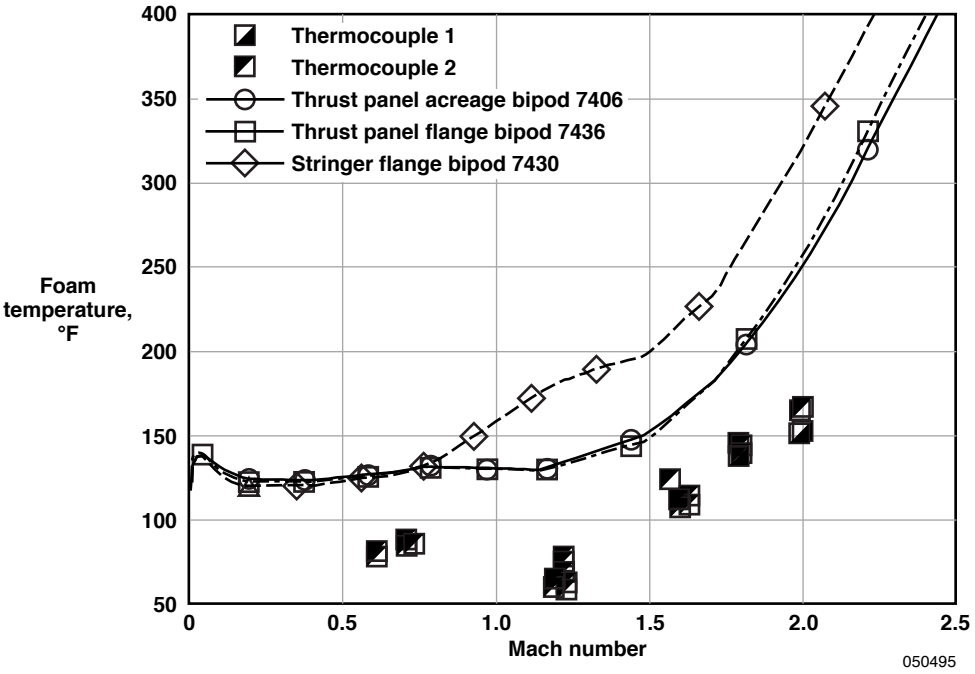

Figure 19. Comparison of foam temperatures from the Lifting Insulating Foam Trajectory flight test and shuttle ascent.

Divot Ejection

Of the 42 shuttle foam divot ejections that were attempted in flight, 36 resulted in successfully ejected divots. In addition, two partial divot ejections occurred in which fractured pieces of foam (rather than a whole divot) separated from the sheet. Table 5 summarizes the divot ejection results.

THIS PAGE INTENTIONALLY LEFT BLANK

Table 5. Flight test divot sizes.

Flight No.	Mach number	Divot	Divot width, in.	Divot radius 1 (R1), in.	Divot radius 2 (R2), in.	R1/R2	Divot average radius, in.
270	1.23	H	0.30	1.0520	0.7295	1.44	0.891
271	1.63	H	0.30	0.9560	0.6195	1.54	0.788
272	1.79	H	0.30	0.9475	0.7450	1.27	0.846
277	1.60	H	1.30	0.7585	1.0170	0.75	0.888
274	1.20	E	0.56	1.1380	1.5115	0.75	1.325
275	1.22	E	0.56	0.9220	1.4055	0.66	1.164
276	1.99	E	0.56	1.1280	1.4875	0.76	1.308
269	0.72	B	1.30	2.0460	1.7970	1.14	1.922
270	1.22	B	1.30	2.0080	2.1390	0.94	2.074
271	1.63	B	1.30	2.1235	2.2035	0.96	2.164
272	1.79	B	1.30	2.1370	2.0770	1.03	2.107
277	1.60	B	1.30	2.0640	1.9525	1.06	2.008
269	0.71	C	1.67	2.3680	2.1690	1.09	2.269
270	1.22	C	1.67	2.4435	2.4195	1.01	2.432
271	1.63	C	1.67	2.4975	2.6120	0.96	2.555
272	1.80	C	1.67	2.5565	2.7075	0.94	2.632
277	1.60	C	1.67	2.6570	2.6165	1.02	2.637
274	1.19	D	1.67	2.7810	2.7105	1.03	2.746
275	1.22	D	1.67	2.4625	2.4750	0.99	2.469
276	1.99	D	1.67	2.6170	2.4375	1.07	2.527
269	0.61	I	1.67	2.2545	1.7920	1.26	2.023

Table 5. Continued.

Largest divot diameter (*L*), in.	Divot thickness (*HT*), in.	*L*/*HT*	Divot angle, deg	Divot volume, ft^3	Divot weight, lb	Divot area, ft^2
1.78	0.65	2.74	41.3	0.00037	0.0008	0.04
1.58	0.65	2.42	45.5	0.00030	0.0006	0.03
1.69	0.65	2.60	43.0	0.00034	0.0007	0.04
1.78	1.00	1.78	76.6	0.00108	0.0023	0.06
2.65	0.83	3.19	38.5	0.00111	0.0023	0.09
2.33	0.83	2.80	43.2	0.00088	0.0019	0.07
2.62	0.83	3.15	38.9	0.00108	0.0023	0.08
3.84	1.00	3.84	38.2	0.00325	0.0069	0.18
4.15	1.00	4.15	35.1	0.00368	0.0078	0.21
4.33	1.00	4.33	33.5	0.00394	0.0083	0.22
4.21	1.00	4.21	34.5	0.00378	0.0080	0.21
4.02	1.00	4.02	36.4	0.00349	0.0074	0.20
4.54	1.11	4.09	37.8	0.00520	0.0110	0.25
4.86	1.11	4.38	34.8	0.00581	0.0123	0.28
5.11	1.11	4.60	32.8	0.00629	0.0133	0.31
5.26	1.11	4.74	31.7	0.00661	0.0139	0.33
5.27	1.11	4.75	31.6	0.00663	0.0140	0.33
5.49	1.11	4.95	30.2	0.00708	0.0150	0.35
4.94	1.11	4.45	34.2	0.00596	0.0126	0.29
5.05	1.11	4.55	33.3	0.00618	0.0131	0.30
4.05	1.11	3.65	43.0	0.00436	0.0092	0.21

Table 5. Continued.

Flight No.	Mach number	Divot	Divot width, in.	Divot radius 1 (R1), in.	Divot radius 2 (R2), in.	R1/R2	Divot average radius, in.
270	1.22	A	1.68	2.1955	2.3200	0.95	2.258
271	1.63	A	1.68	2.2180	2.3170	0.96	2.268
272	1.79	A	1.68	2.2350	2.3890	0.94	2.312
277	1.60	A	1.68	2.3125	2.2055	1.05	2.259
274	1.21	F	1.68	2.2390	2.1680	1.03	2.204
275	1.22	F	1.68	2.2745	2.2460	1.01	2.260
276	2.00	F	1.68	2.2835	2.1905	1.04	2.237
269	0.61	G	1.68	1.9425	2.0020	0.97	1.972
270	1.23	G	1.68	2.2460	2.2310	1.01	2.239
271	1.63	G	1.68	2.2460	2.2810	0.98	2.264
272	1.79	G	1.68	2.0845	2.0815	1.00	2.083
277	1.60	G	1.68	2.3595	2.2975	1.03	2.329

Table 5. Concluded.

Largest divot diameter (L), in.	Divot thickness (HT), in.	L/HT	Divot angle, deg	Divot volume, ft^3	Divot weight, lb	Divot area, ft^2
4.52	0.95	4.75	33.8	0.00443	0.0094	0.24
4.54	0.95	4.77	33.6	0.00446	0.0094	0.24
4.62	0.95	4.87	32.8	0.00460	0.0097	0.25
4.52	0.95	4.76	33.8	0.00444	0.0094	0.24
4.41	0.95	4.64	34.9	0.00427	0.0090	0.23
4.52	0.95	4.76	33.8	0.00444	0.0094	0.24
4.47	0.95	4.71	34.2	0.00437	0.0092	0.24
3.94	0.95	4.15	40.0	0.00360	0.0076	0.19
4.48	0.95	4.71	34.2	0.00437	0.0092	0.24
4.53	0.95	4.77	33.7	0.00445	0.0094	0.24
4.17	0.95	4.39	37.4	0.00391	0.0083	0.21
4.66	0.95	4.90	32.5	0.00465	0.0098	0.26

All of the divot ejections were captured with high-speed digital video at 2,000 pps. Figures 20 and 21 show composite digital video frame captures of divot ejections from flight 9 at Mach 1.99, an altitude of 48,240 ft (14,704 m), and a dynamic pressure of 730 lbf/ft^2 (34,953 N/m^2). Figure 20(a) shows the forward camera view, and figure 20(b) shows the aft camera view. The conical frustum-shaped divot was cleanly ejected from the AFTF and trimmed with its small diameter facing upstream.

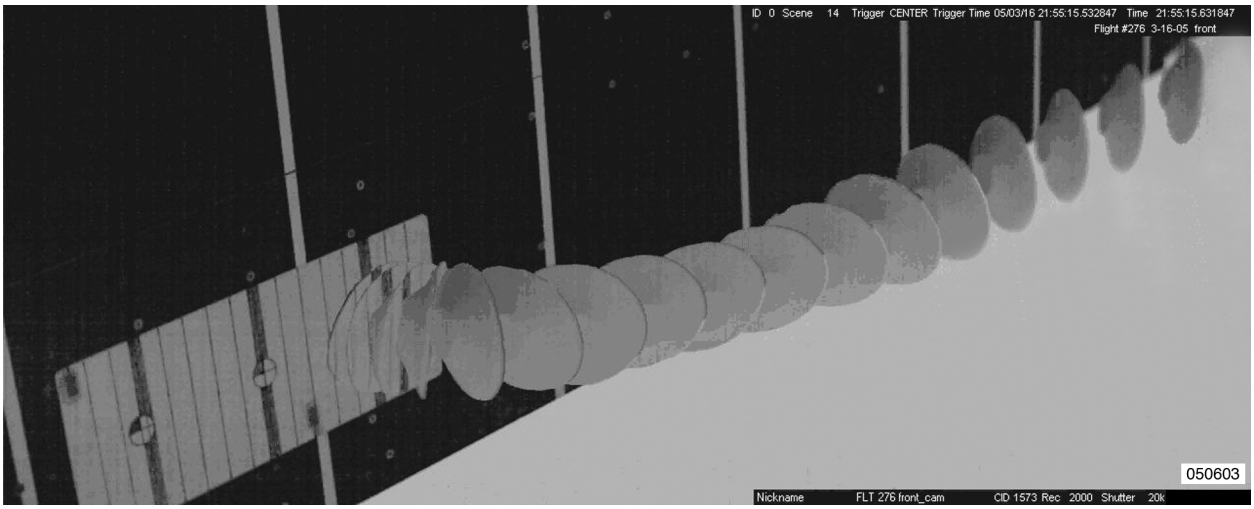

(a) Forward camera view (looking downstream).

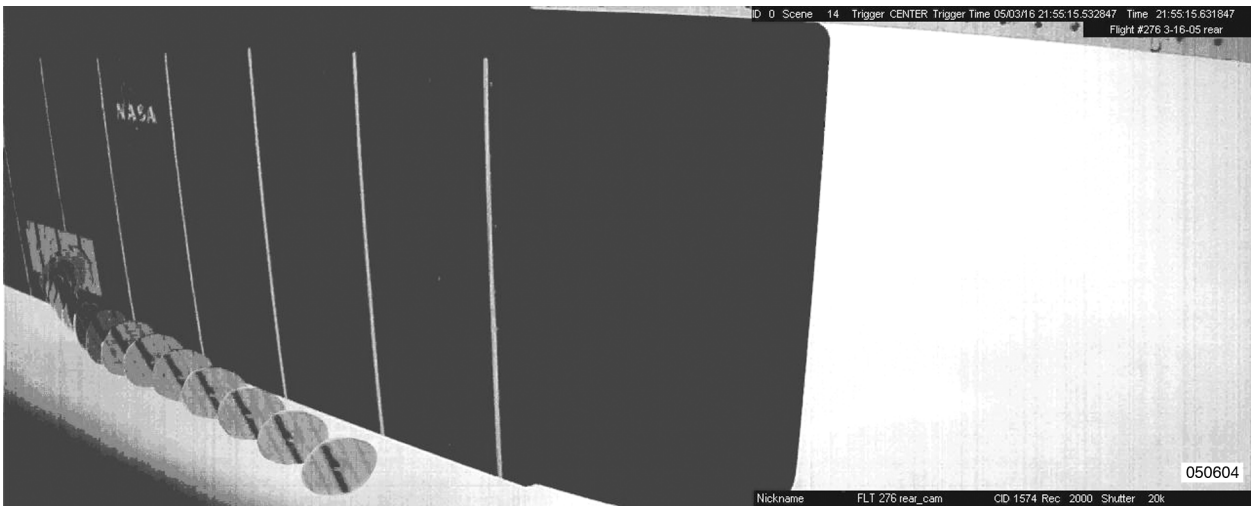

(b) Aft camera view (looking upstream).

Figure 20. Composite digital video frame captures (at 2,000 pps) of divot ejections.

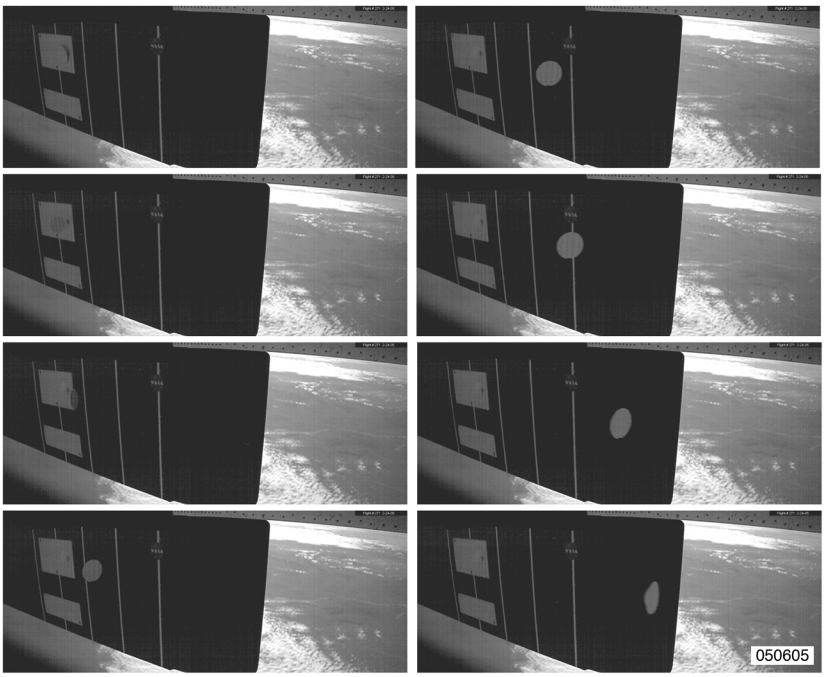

Figure 21. Composite digital video frame captures (at 2,000 pps) of divot ejections, forward camera view.

Figures 22 and 23 show examples of the shuttle foam panels after the in-flight divot ejection. Figure 22 shows the foam panels in the AFTF bays 3A and 3B after LIFT flight 4 at Mach 1.63, an altitude of 40,200 ft (12,253 m), and a dynamic pressure of 720 lbf/ft^2 (34,474 N/m^2). All six divots were successfully ejected. Figure 23 shows a postflight close-up picture of the shuttle foam panel 3A from LIFT flight 3 at Mach 1.2, an altitude of 29,000 ft (8,839 m), and a dynamic pressure of 700 lbf/ft^2 (33,516 N/m^2).

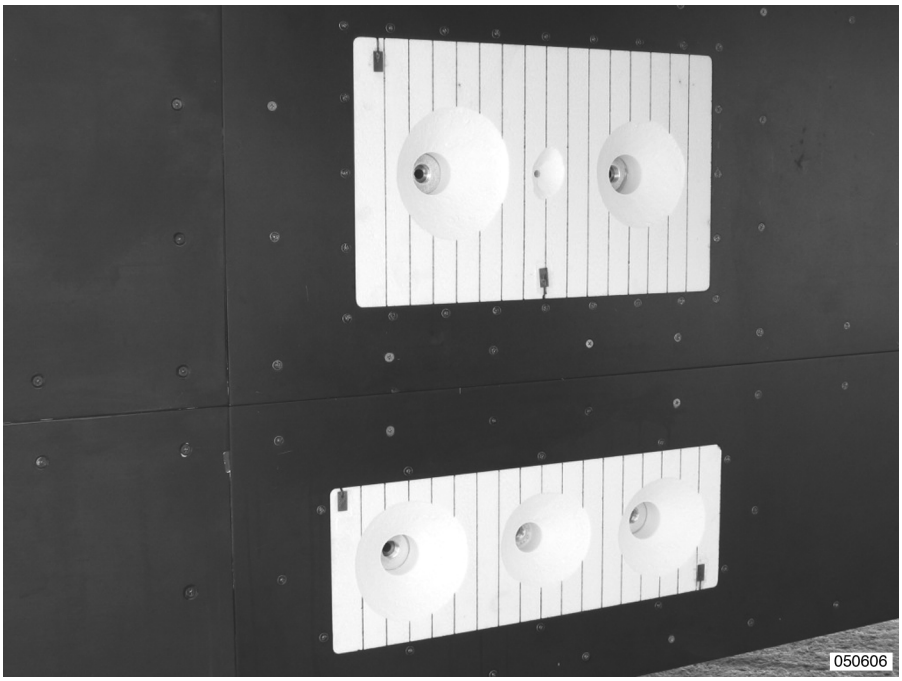

Figure 22. Foam panels after the in-flight divot ejection.

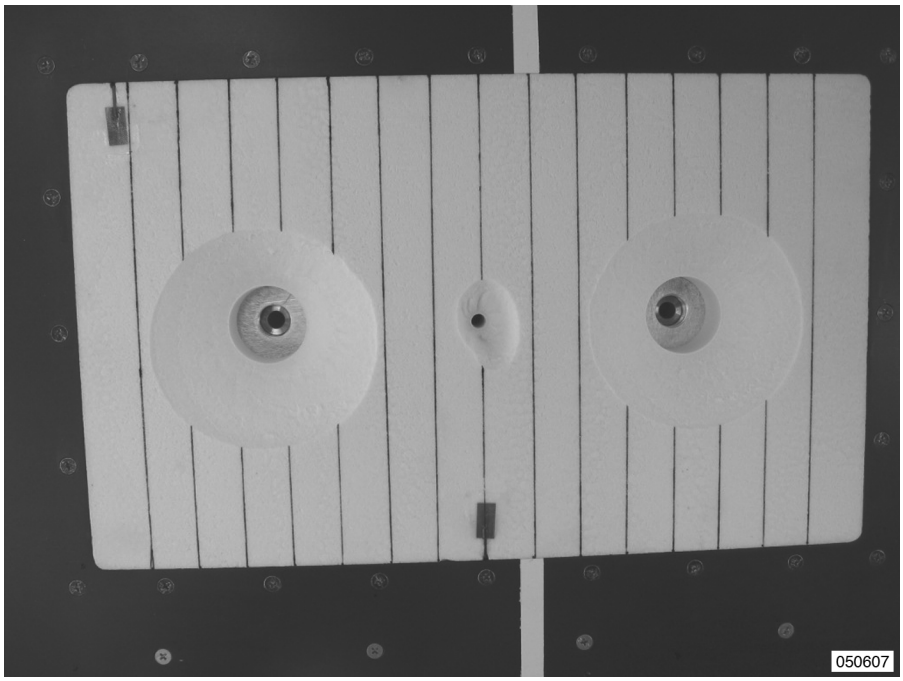

Figure 23. Postflight close-up view of foam panel.

Figure 24 shows the pressure required to cleanly eject divots from the foam sheets as a function of divot void diameter. The divot ejection pressure is shown as a gauge pressure defined as the difference between the absolute pressure behind the divot and the free-stream static pressure on the external surface of the divot. The figure shows both ground and flight test data. The ejection pressure did not appear to affect the divot geometry.

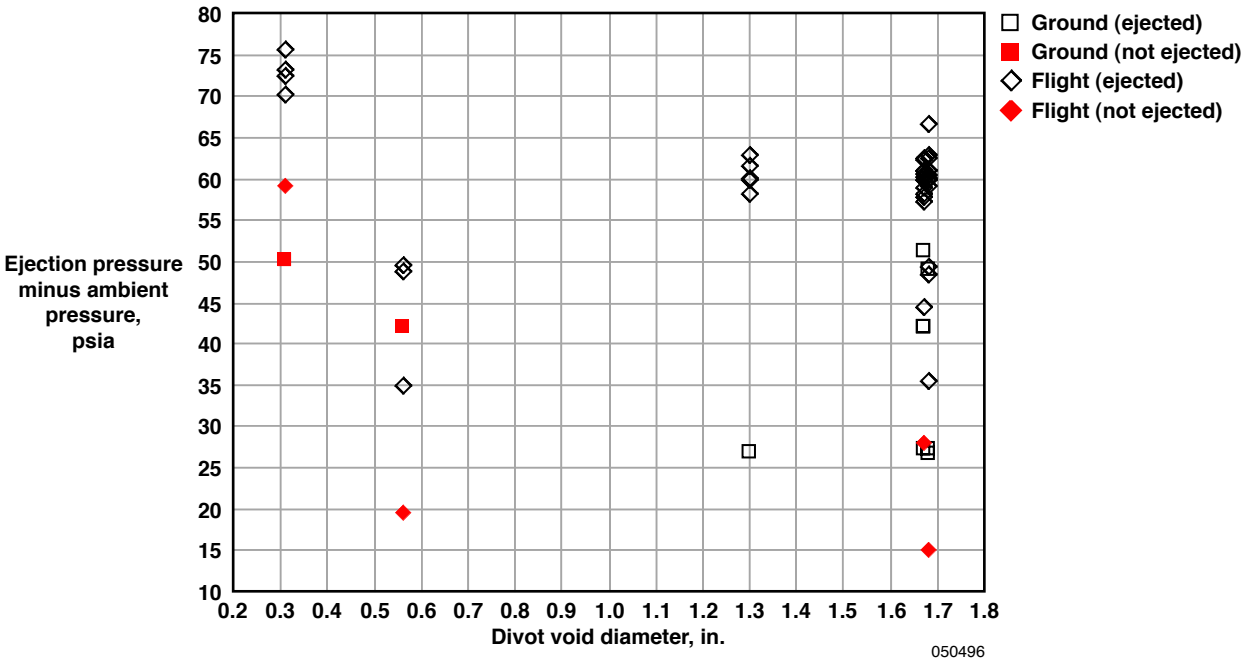

Figure 24. Divot ejection pressure as a function of divot void diameter.

Divot Structural Integrity

Thirty-six divots survived the aerodynamic deceleration associated with ejection into the flow field. Of the three divots generated from the lowest successful ejection pressure, two rotated back into the foam sheet. As a result of this recontact with the sheet, these divots fractured into several pieces.

Divot Shape and Size

The ejected divots had a conical frustum shape, in which the larger and smaller diameters are defined as the divot diameter and void diameter, respectively. Figure 25 defines the divot geometry. Most of the ejected divots had a near circular shape, except for the divots obtained from the smallest void (see table 2, divot case 1). The smallest voids, nominally less than 1/2 in. (12.7 mm) in diameter, tended to produce elliptical outer surface divots.

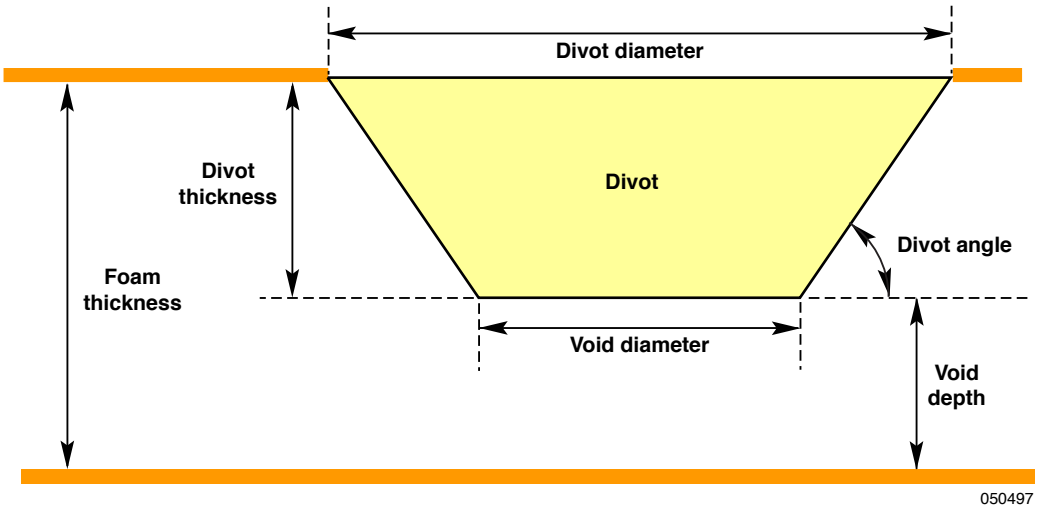

Figure 25. Definition of divot geometry.

Figure 26 shows the divot aspect ratio, defined as the largest divot diameter, *L*, divided by divot thickness, *HT*, as a function of divot thickness. Divot data are presented for the F-15B flight test and for various ground tests. The aspect ratios of the divots obtained from the flight tests all were smaller than those obtained from ground tests. In the ground tests, the outer and inner foam surface temperatures were matched to the shuttle conditions, hot wall outer surface and cold wall inner surface. The outer temperature of the flight test foam was colder and the inner temperature was warmer than the temperatures of the ground test foam. This mismatch in foam temperature resulted in different divot wall angles between ground and flight. Table 5 presents details of the flight test divot sizes.

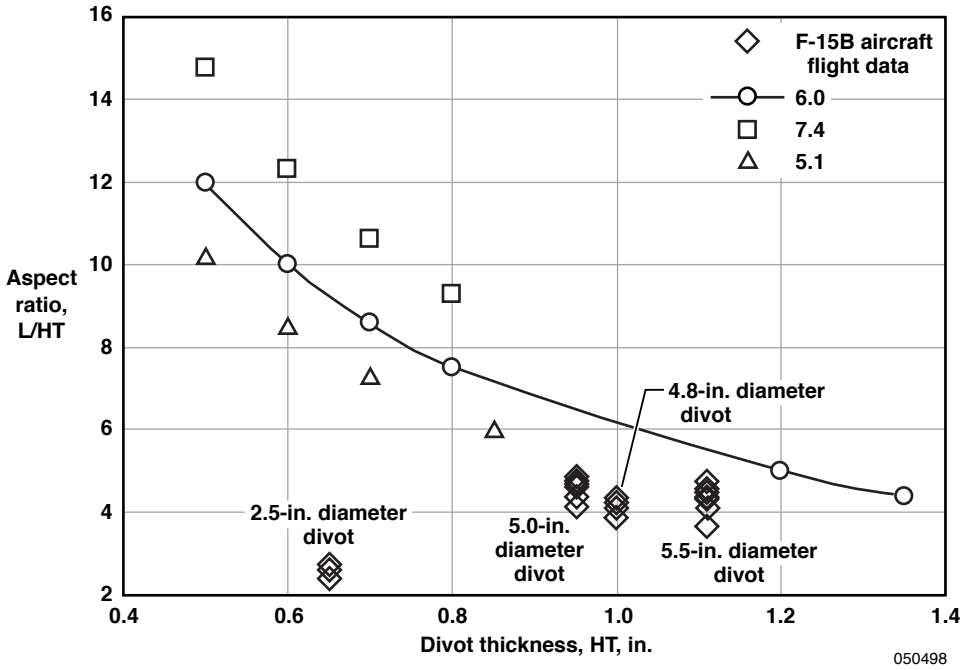

Figure 26. Divot aspect ratio as a function of divot thickness.

Divot Aerodynamic Stability

The DTA assumes three potential aerodynamic models for the divot shape: the static or high drag model in which the divot trims with its small diameter into the wind, the nominal drag model in which the divot oscillates back and forth about its static trim point, and the tumble or low drag model in which the divot tumbles. The static and tumbling models are considered to bound the potential deceleration of the divot when it is released into the flow field.

As shown in figure 20, the divots tended to trim with their small diameters forward (facing into the wind). All 31 of the supersonic divots trimmed. Of the five subsonic divots, two tumbled after one oscillation. Figure 27 shows the situation in which the divot trimmed with its large diameter facing upstream during flight 10 at Mach 1.6, an altitude of 36,124 ft (11,011 m), and a dynamic pressure of 848 lbf/ft^2 (40,602 N/m^2). The divot did not cleanly eject from the AFTF; instead, the downstream edge of the divot fractured into several smaller pieces. The resulting asymmetrical divot was ejected and passed through a yawing oscillation before trimming with its large diameter facing upstream. The estimated divot dimensions are 5.3 by 1.7 by 1.1 in. (0.135 by 0.0432 by 0.0279 m), with a mass of 0.014 lbm (0.00635 kg).

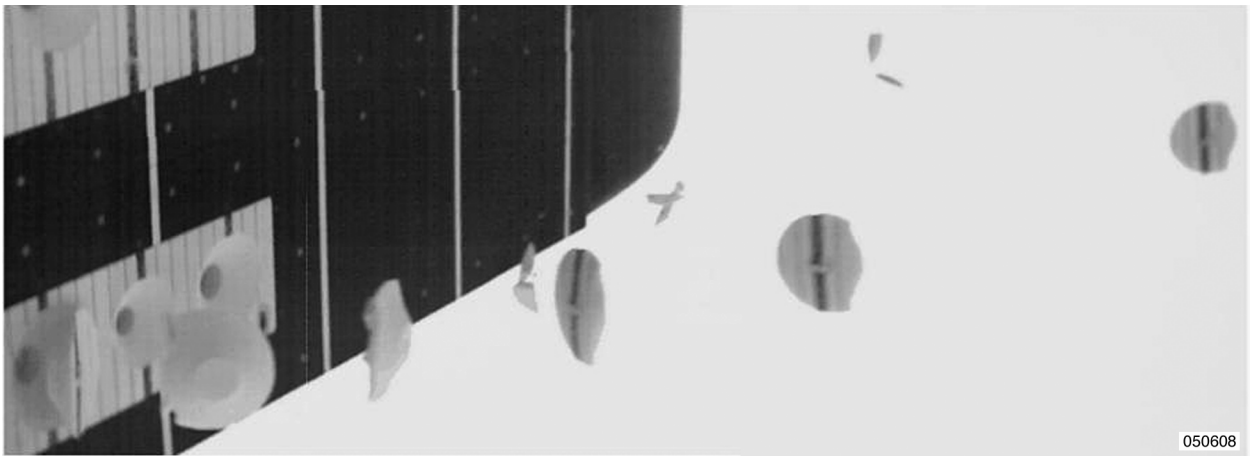

Figure 27. Composite digital video frame captures of divot ejection, forward camera view looking aft at 2,000 pps, time and number of frames from ejection (divot C).

Divot Photogrammetry and Trajectories

Standard photogrammetry analysis techniques were used to estimate the divot trajectories from the high-speed digital video. Photogrammetry uses photographic images to obtain measurements of position and rotation. Velocity can be calculated by differentiating the spatial coordinates with respect to time. The divot spatial position, rotation, and velocity were estimated for the in-flight ejections. Reference 7 presents details and results of the photogrammetry technique.

Figure 28 shows trajectories calculated from the F-15B flight data by means of photogrammetry and from a 1-DOF DTA prediction. Downrange distance is plotted as a function of time from ejection. Three 1-DOF trajectories are shown based on the assumed divot stability-drag model: the nominal drag model in which the divot oscillates about its static trim point, the static or high drag model in which the divot trims with its small diameter facing upstream, and the tumble or low drag model in which the divot tumbles. The trajectory based on the nominal drag model appears to most closely match the flight data. The trajectories based on the static (high drag) and tumble (low drag) models appear to properly bound the nominal trajectory and flight data.

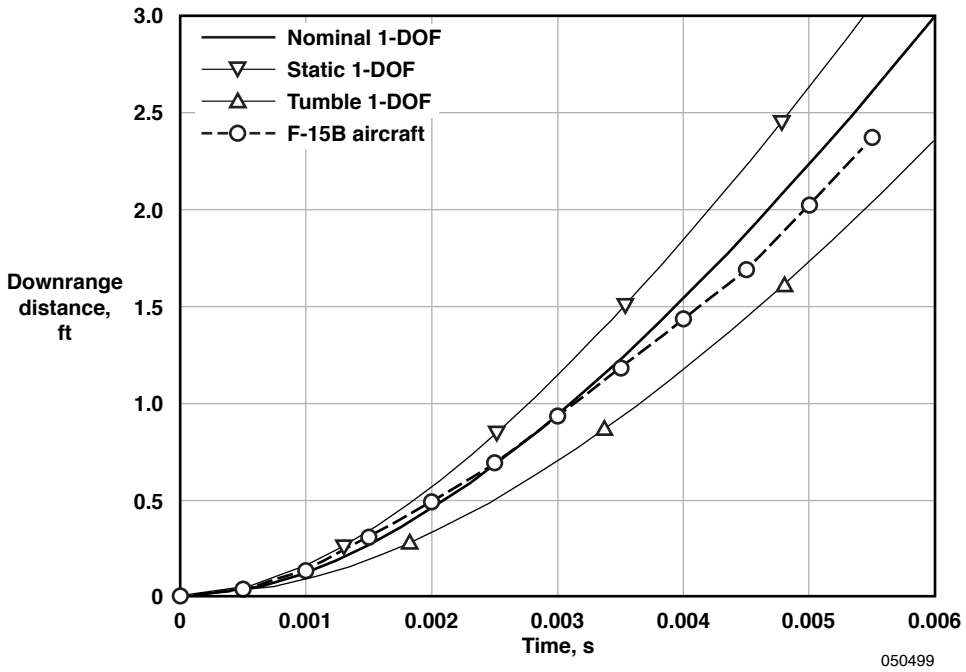

Figure 28. Comparison of F-15B flight data with one-degree-of-freedom prediction (flight 10, divot C, Mach 1.6, altitude of 36,120 ft, and dynamic pressure of 850 lbf/ft^2).

CONCLUDING REMARKS

Flight tests were conducted on the NASA F-15B aircraft to assess the structural survivability of Space Shuttle external tank foam debris or "divots" in a real flight environment. Divots were ejected from foam sheets mounted on the side of the Aerodynamic Flight Test Fixture, which was carried underneath the F-15B aircraft. Divots were ejected at subsonic, transonic, and supersonic speeds to Mach 2. A total of 10 divot ejection test flights were flown with 36 successful in-flight divot ejections. The divot ejection flight conditions matched the altitude and Mach number at discrete points along the shuttle ascent trajectory. High-speed digital video was used to capture the divot ejections and trajectories.

The divots remained structurally intact if they were cleanly ejected, that is, if the divots did not recontact with the foam sheets or Aerodynamic Flight Test Fixture. In general, the cleanly ejected divots had a nearly circular planform shape. The aspect ratios of the divots obtained in flight were smaller than those obtained from ground tests. The difference in aspect ratio is the result of a mismatch in wall temperature conditions between the flight and ground tests. After ejection, the conical frustum-shaped divots tended to trim with their large diameters facing upstream. All 31 of the supersonically ejected divots trimmed. Of the five divots ejected at subsonic speeds, two tumbled after one oscillation. The flight data were compared with debris transport analysis predictions of the divot trajectories for various divot drag models. Photogrammetric techniques were used to estimate divot position, orientation, and speed from the flight data. The divot trajectories based on the nominal drag model of the debris transport analysis most closely matched the flight data.

REFERENCES

1. Columbia Accident Investigation Board: Report, Volume 1, Aug. 2003.

2. Richwine, David M., *F-15B/Flight Test Fixture II: A Test Bed for Flight Research*, NASA TM-4782, 1996.

3. Meyer, Robert R., Jr., *A Unique Flight Test Facility: Description and Results*, NASA TM-84900, 1982.

4. Corda, Stephen, M. Jake Vachon, Nathan Palumbo, Corey Diebler, Ting Tseng, Anthony Ginn, and David Richwine, *The F-15B Propulsion Flight Test Fixture: A New Flight Facility for Propulsion Research*, NASA TM-2001-210395, 2001.

5. Palumbo, Nathan, Timothy R. Moes, and M. Jake Vachon, *Initial Flight Tests of the NASA F-15B Propulsion Flight Test Fixture*, NASA TM-2002-210736, July 2002.

6. Tseng, Ting, Matthew Reaves, and Kendall Mauldin, *High Speed Video for Airborne Instrumentation Application* (to be published).

7. Smith, Mark S., *Photogrammetric Trajectory Estimation of Foam Debris Ejected from an F-15 Aircraft*, NASA TM-2006-213675, 2006.

8. *Standard General Requirements for Safe Design and Operation of Pressurized Missile and Space Systems*, MIL-STD-1522A, 1984.

9. Ko, William L., *Impacts of Space Shuttle Thermal Protection System Tile on an F-15 Aircraft Vertical Tail*, NASA TM-85904, 1985.

10. Hoerner, Sighard F., *Fluid-Dynamic Drag: Practical Information on Aerodynamic Drag and Hydrodynamic Resistance*, Dr.-Ing. S. F. Hoerner, Midland Park, New Jersey, 1965.

REPORT DOCUMENTATION PAGE

Form Approved
OMB No. 0704-0188

1. REPORT DATE *(DD-MM-YYYY)*	2. REPORT TYPE	3. DATES COVERED *(From - To)*
28-06-2006	Technical Memorandum	

4. TITLE AND SUBTITLE
The F-15B Lifting Insulating Foam Trajectory (LIFT) Flight Test

5a. CONTRACT NUMBER

5b. GRANT NUMBER

5c. PROGRAM ELEMENT NUMBER

6. AUTHOR(S)
Corda, Stephen, Whiteman, Donald, Tseng, Ting,
and Machin, Ricardo

5d. PROJECT NUMBER

5e. TASK NUMBER

5f. WORK UNIT NUMBER

7. PERFORMING ORGANIZATION NAME(S) AND ADDRESS(ES)
NASA Dryden Flight Research Center
P.O. Box 273
Edwards, California 93523-0273

8. PERFORMING ORGANIZATION REPORT NUMBER
H-2627

9. SPONSORING/MONITORING AGENCY NAME(S) AND ADDRESS(ES)
National Aeronautics and Space Administration
Washington, DC 20546-0001

10. SPONSORING/MONITOR'S ACRONYM(S)
NASA

11. SPONSORING/MONITORING REPORT NUMBER
NASA/TM-2006-213674

12. DISTRIBUTION/AVAILABILITY STATEMENT
Unclassified -- Unlimited
Subject Category 015 Availability: NASA CASI (301) 621-0390 Distribution: Standard

13. SUPPLEMENTARY NOTES
Corda, Whiteman, Tseng, Dryden Flight Research Center; Machin, Johnson Space Center
An electronic version can be found at the NASA Dryden Flight Research Center Web Site, under Technical Reports.

14. ABSTRACT

A series of flight tests has been performed to assess the structural survivability of space shuttle external tank debris, known as divots, in a real flight environment. The NASA F-15B research test bed aircraft carried the Aerodynamic Flight Test Fixture configured with a shuttle foam divot ejection system. The divots were released in flight at subsonic and supersonic test conditions matching points on the shuttle ascent trajectory. Very high-speed digital video cameras recorded the divot trajectories. The objectives of the flight test were to determine the structural survivability of the divots in a real flight environment, assess the aerodynamic stability of the divots, and provide divot trajectory data for comparison with debris transport models. A total of 10 flights to Mach 2 were completed, resulting in 36 successful shuttle foam divot ejections. High-speed video was obtained at 2,000 pictures per second for all of the divot ejections. The divots that were cleanly ejected remained structurally intact. The conical frustum-shaped divots tended to aerodynamically trim in both the subsonic and supersonic free-stream flow.

15. SUBJECT TERMS
Divot Aerodynamics, F-15 Flight Test Fixture, Foam Divot, Photogrammetry, Space Shuttle External Tank

16. SECURITY CLASSIFICATION OF:			17. LIMITATION OF ABSTRACT	18. NUMBER OF PAGES	19a. NAME OF RESPONSIBLE PERSON
a. REPORT	b. ABSTRACT	c. THIS PAGE			STI Help Desk (email: help@sti.nasa.gov)
					19b. TELEPHONE NUMBER *(Include area code)*
U	U	U	UU	58	(301) 621-0390